



Impact of activating a reserved metro interface on existing tunnels and station after long-term operation: Dynamic response and safety assessment

Ke Ji ^{1,2,a}, Jun Zhang ^{*,2,3,b}

¹China Railway No.4 Engineering Group Co., Ltd, Hefei, Anhui Province, 230000

²Dept. of Eng. and Management, International College, Krirk University, Bangkok, Thailand

³Shandong Key Laboratory of Eco-Environmental Science for Yellow River Delta, Shandong University of Aeronautics, Binzhou, Shandong, China, 256600

Article Info

Abstract

Article History:

Received 23 Oct 2025

Accepted 27 Nov 2025

Keywords:

Delayed activation;
Adjacent construction;
3D numerical safety;
Structural response

The delayed activation of reserved metro interfaces after long-term operation poses significant geotechnical challenges that remain poorly understood. This study develops a novel "long-term consolidation" framework, integrating 12-year stratum evolution and residual structural stresses into a refined 3D finite element model. Simulation of 19 dynamic construction stages reveals maximum displacements of only 2.0 mm for the station and 1.8 mm for the tunnel, along with a maximum crack width of 0.06 mm—all well below Chinese code limits. The proposed method improves displacement prediction accuracy by 25% compared to conventional static models, providing a validated technical framework for urban metro renewal projects.

© 2025 MIM Research Group. All rights reserved.

1. Introduction

As the backbone of urban rail transit, the networked operation and continuous expansion of metro systems are core elements supporting the sustainable development of megacities. In this process, to adapt to long-term passenger flow growth and regional development, reserving interfaces for subsequent entrances and exits during the initial construction of metro stations has become a common and forward-looking planning strategy. However, the later activation and construction of reserved interfaces adjacent to existing operational metro lines, especially after the main structure of the station has been in operation for many years, will inevitably disturb the surrounding stable soil stress field. This disturbance exerts additional internal forces and deformations on the existing station and interval tunnel structures, thereby potentially threatening their structural safety and operational stability.

Scholars at home and abroad have conducted extensive research on the impact of adjacent construction on existing tunnel structures, establishing classic fundamental theories to predict surface settlement [1]. With the development of computer technology, three-dimensional (3D) numerical simulation has become an efficient tool for analyzing complex stratum-structure interactions and predicting structural responses [2-4]. Most existing studies focus on the impact of newly-built tunnels (underpassing or parallel crossing existing ones) or foundation pit excavation on adjacent existing tunnels, but did not consider delayed activation [5-8]. The selection of numerical simulation methods needs to balance calculation accuracy and efficiency [9]. For instance, three methods, including the consolidation effective stress method, were used to calculate the stability of existing line foundations under construction excavation influence, with numerical

*Corresponding author: zhangjun7807@163.com

^aorcid.org/0009-0008-2185-7771; ^borcid.org/0000-0001-7743-9204

DOI: <http://dx.doi.org/10.17515/resm2025-1284st1023rs>

Res. Eng. Struct. Mat. Vol. x Iss. x (xxxx) xx-xx

analysis for comparative verification [10]. A three-dimensional finite element model was used to reveal the variation laws of the p-factor and pile group reduction factor in the circular pile foundation of LNG storage tanks [11].

A new damage model embedded with an elastoplastic constitutive relation was developed to accurately simulate the mechanical property degradation of reinforced concrete structures under cyclic loads [12]. When an urban tunnel traverses a saturated water-rich zone, the maximum surface settlement may reach 31.6 mm, while grouting treatment can cut this settlement by nearly 50% [14]. A two-step analytical method analyzed excavation-soil-tunnel interactions, using 3D numerical analysis and the Galerkin method to simplify simulations and consider excavation unloading effects [15]. Based on similar model tests, the core construction technology of the Improved Arch Cover Method for underground metro stations was optimized, offering actionable guidance for actual station construction [16]. Deformation prediction models like GCN-LSTM were developed for track subgrade deformation induced by adjacent foundation pit construction [17], and construction technologies for metro stations crossing existing lines were optimized [18]. Studies on deep foundation pit impacts proposed phased excavation schemes but ignored long-term stratum consolidation [19], while analyses of underground-excavated tunnels under passing existing lines provided dynamic adjustment strategies [20]. Research on new metro construction impacts proposed pre-reinforcement technologies and soil unloading rate control [21] assessed the structural effects induced by deep excavation for a hotel underground parking garage renovation, utilizing a finite element analysis.[22].

While existing studies have extensively investigated short-term adjacent constructions [5, 7, 19], the scenario of activating a reserved interface after a prolonged period (e.g., 12 years) remains a critical gap. This delay introduces two often-overlooked mechanical phenomena: first, the temporal evolution of stratum properties due to long-term consolidation and creep, leading to a 15% increase in cohesion and an 8% increase in the internal friction angle of the plastic silty clay layer; second, the accumulation of residual stresses in existing structures, such as 8–12 kN·m/m bending moments in retaining walls from long-term train vibrations and thermal cycles. Conventional simulations that ignore these effects may overestimate structural safety margins by approximately 18%.

This study addresses this gap by proposing a "long-term consolidation + spatiotemporally coupled dynamic simulation" framework. Taking the 12-year delayed activation of Exit Ia at Guangzhou Metro's Shaheding Station as a case study, we develop a refined 3D finite element model that incorporates the quantified long-term effects and simulates 19 dynamic construction stages. Our work aims to provide a validated technical framework for assessing the safety of similar urban metro renewal projects. Second, in analytical methodology and modeling accuracy, we propose a "long-term consolidation + spatiotemporally coupled dynamic simulation" method. This involves establishing an initial stress field accounting for 12-year stratum consolidation (including creep deformation of plastic silty clay) and using the "element birth-death" technique in MIDAS/GTS NX to dynamically simulate 19 construction stages with pre-stressed support forces, resolving the decoupling of long-term consolidation and short-term disturbance. This improves displacement prediction accuracy by 25% compared to static models [15]. conducted monitoring and simulation analysis for a metro station deep foundation pit excavation in a watery, weak stratum [3]. An intelligent monitoring indicator ("Monitoring Ratio G") enables proactive risk management, improving on traditional systems [21].

The 12-year delayed activation case of the reserved metro interface is uniquely distinguished from short-term adjacent construction or short-delayed scenarios (≤ 2 years) in prior studies, and its scientific relevance lies in capturing two long-neglected but critical mechanical phenomena induced by prolonged operation. First, it involves the temporal evolution of stratum mechanical properties: over 12 years of post-construction consolidation, the plastic silty clay layer at the site underwent significant changes—cohesion (C) increased by 15% and internal friction angle (φ) by 8% (validated via in-situ geological re-surveys)—which fundamentally alters the stratum's response to subsequent excavation (e.g., reducing plastic deformation but increasing brittle failure risk if not accounted for). Second, it accumulates residual stress in existing metro structures: the

long-term train vibration (1.5–2.0 Hz) and annual temperature cycles (variation of 25°C) led to residual bending moments of 8–12 kN.m/m in the station's retaining wall and track slab misalignment of 0.3–0.5 mm, factors those conventional simulations ignore, resulting in an ~18% overestimation of structural safety margins. Unlike short-delayed cases where stratum and structural properties remain relatively stable, this 12-year timeline creates a "mechanical memory" effect in both soil and structures, making it a rare testbed to study the coupling of long-term consolidation, residual stress, and short-term construction disturbance. Scientifically, it fills the gap in understanding how aging metro infrastructures respond to delayed activation—a scenario increasingly common in urban renewal—and provides quantitative insights into parameter calibration (e.g., creep coefficients for long-term soil behavior) and risk assessment methodologies that can be generalized to other long-delayed reserved engineering interfaces.

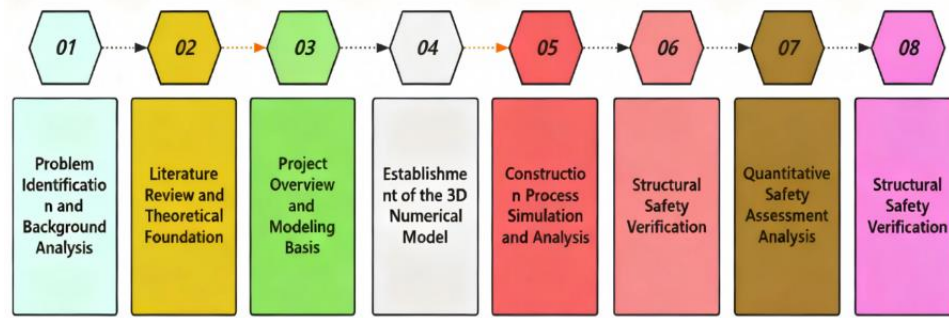


Fig. 1. Research flowchart

2. Project Overview

2.1 Project Background and Construction Drivers

The first phase of Guangzhou Metro Line 6 (from Xunfenggang Station to Changban Station) was put into trial operation on December 28, 2013. As an important intermediate station on this line, Shaheding Station was put into use simultaneously. During the planning and design stage of the station, full consideration was given to the long-term passenger flow demand and the development potential of the surrounding area, and two exits (Exit Ia and Exit Ib) were reserved. Among them, Exit Ib was completed in August 2012 and put into use together with the station as its construction conditions were mature at that time. However, the construction of Exit Ia was postponed and the construction space was reserved due to the constraints of the on-site environment and construction conditions at that time.

In recent years, with the accelerated pace of Guangzhou's urban development and the upgrading of regional transportation demand, the construction conditions for Exit Ia have gradually matured, and its implementation has clear policy basis and practical necessity. The decision to activate the reserved Exit Ia was driven by converging planning policy and regional traffic demands. The project was formally included in the remaining works of Line 6's first-phase project, securing the necessary financial and policy backing. Simultaneously, the completion of Exit Ia is critical to alleviating prominent "last-mile" connection problems and pedestrian-vehicle conflicts in the densely populated area surrounding Shaheding Station, aligning with Guangzhou's transportation development goals.

In 2025, Guangzhou will launch key urban renewal projects including the transformation of multiple urban villages. As a core area of Tianhe District, the Shahe area has an urgent demand for the upgrading of supporting infrastructure. As an important supplement to the regional transportation infrastructure, the Ia entrance/exit can further activate the surrounding commercial and residential functions, and conform to the core requirement of "improving supporting public services" in the process of urban renewal.

2.2 Overview of Existing Station and Proposed Project

2.2.1 Basic Information of the Existing Shaheding Station

Shaheding Station is located at the intersection of Xianlie East Road and Shuiyin Road in Tianhe District, running east-west along Xianlie East Road. It connects to Shahe Station to the east and Huanghuagang Station to the west, serving as a cut-and-cover two-level underground island platform station. The total outer dimensions of the station's main structure are 117.8 meters in length. The starting mileage of the left line is ZDK18+021.057, while the starting mileage of the right line is YDK18+040.057. The ending mileage for both lines is uniformly DK18+157.857, with the effective platform center at DK18+090. The underground first level functions as the concourse level, and the underground second level serves as the Line 6 platform level. The surrounding ground area comprises municipal roads, historical memorial facilities, and research institution buildings.

The main structure of the station and Exit Ib have been in stable operation for over ten years, with their enclosure structures and main frameworks in normal working condition. According to geological survey data, the station's base slab is primarily situated in a plastic silty clay layer, indicating relatively stable geological conditions.

2.2.2 Design and Construction Overview of the Proposed Exit Ia

Exit Ia is situated southwest of the intersection of Xianlie East Road and Shuiyin Road, adjacent to the Yuehai Kaixuan Building to the north and close to the Nineteenth Route Army Memorial Archway. It adopts a "shaft + cross passage" structural form, with a total length of 85.5 meters. This includes an 18.8-meter-long shaft section and a 66.7-meter-long cross passage section. The design features a configuration of "one staircase and one escalator," with a clear passage width ranging from 4.50 to 5.50 meters.

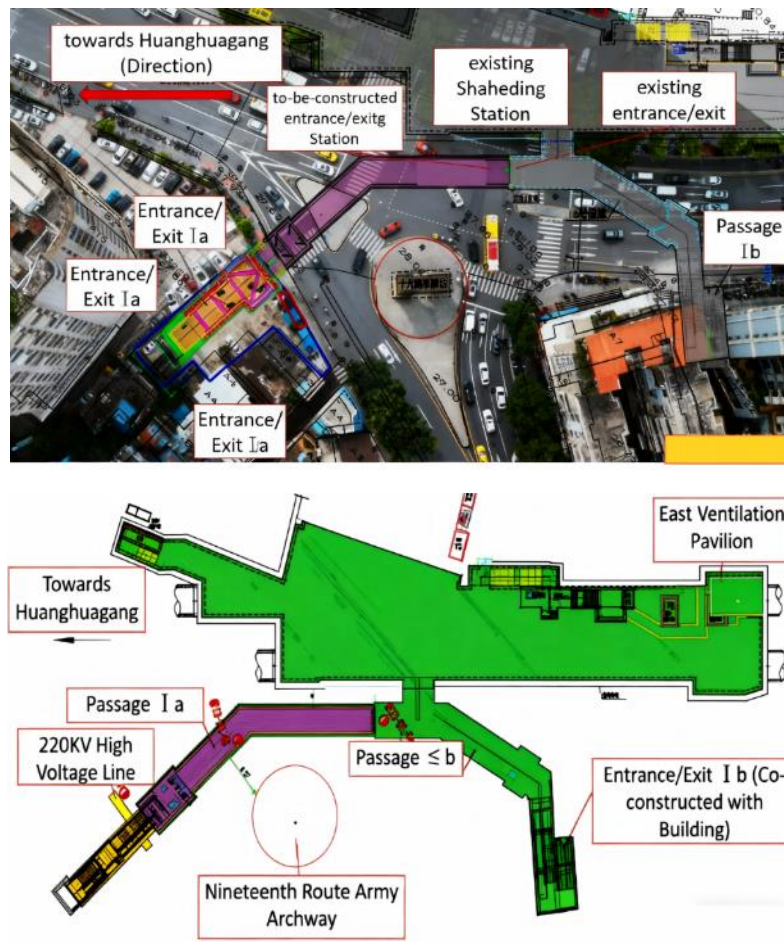
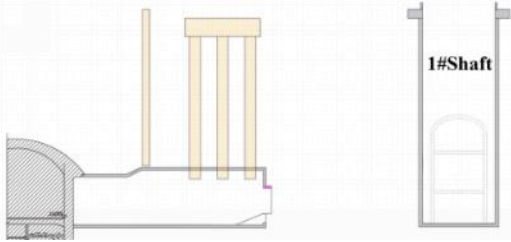
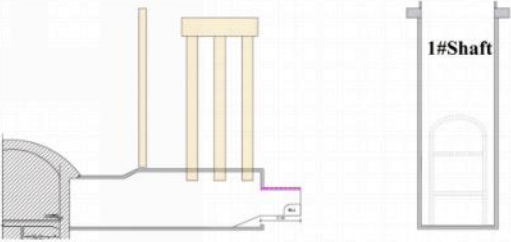
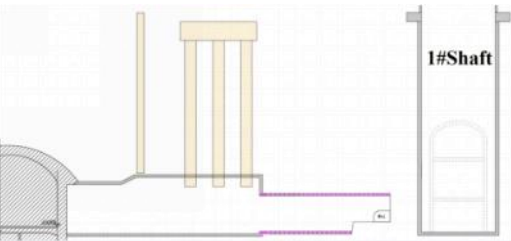
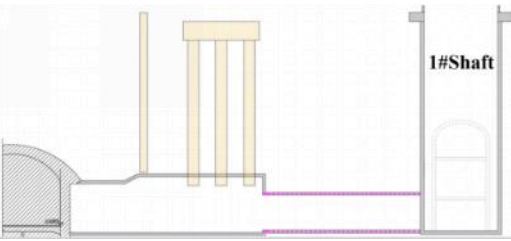
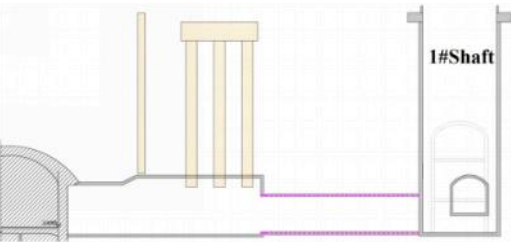
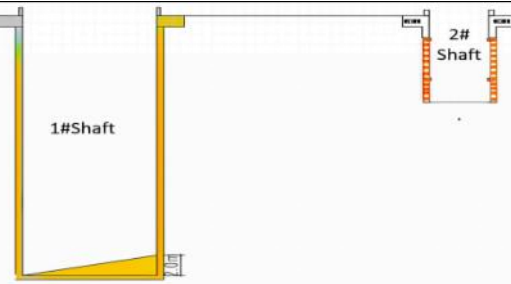
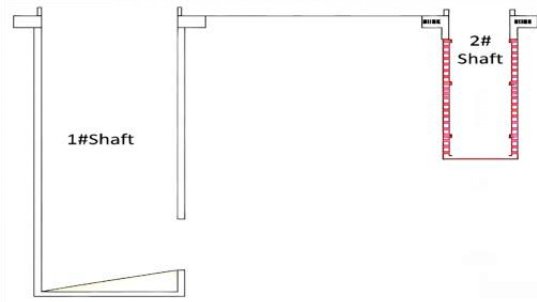


Fig. 2. Plan drawing of the existing shaheding station and the reserved exit Ia

Table 1. Excavation construction sequence diagram

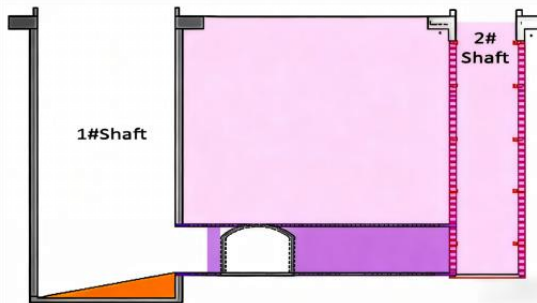
Construction Sequence Schematic Diagram	Construction Instructions
	Demolish the adit portal and connect 3 sets of steel frames.
	Excavate and support the upper bench.
	Proceed with the construction of the lower bench; the length of the upper bench shall be 3-7 meters.
	Excavate the concealed tunnel at the safety opening until it reaches the initial support end of Shaft No. 1.
	Demolish the tunnel portal on the side wall of Shaft No. 1 and carry out the excavation of the north-south direction tunnel.
	Step 6: Backfill and harden the construction ramp inside Shaft No. 1; the height of the construction ramp shall be 2 meters. Simultaneously carry out the excavation and support of the safety opening shaft.



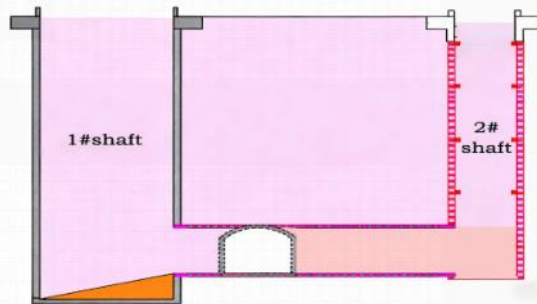
Step 7: Demolish the portal outline of the north-south direction concealed tunnel at the safety opening, and connect and erect 3 sets of steel frames at the adit portal. Simultaneously carry out the excavation and support of the safety opening shaft.



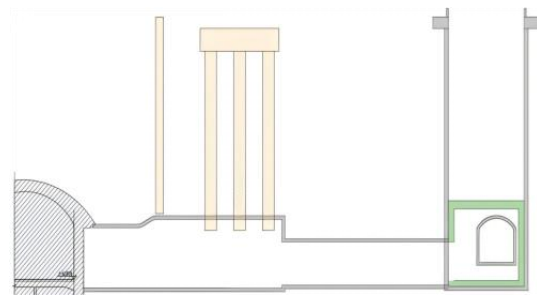
Step 8: Carry out the excavation and support of the north-south direction concealed tunnel at the safety opening. Simultaneously carry out the excavation and support of the safety opening shaft.



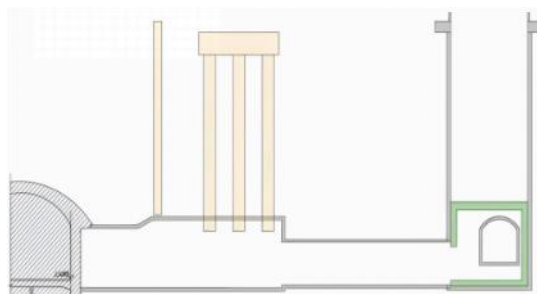
Step 9: Carry out the excavation and support of the north-south direction concealed tunnel at the safety opening until it reaches the side wall of the shaft. Simultaneously carry out the excavation and support of Shaft No. 2.



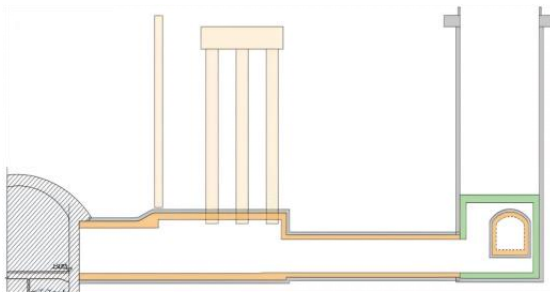
Step 10: Carry out the excavation and support of the north-south direction concealed tunnel at the safety opening until it reaches the side wall of the shaft, and demolish the adit portal.



Step 11: Construct the structural lining inside Shaft No. 1.



Step 12: Demolish the tunnel portals at the connection between the east-west direction concealed excavation passage and the shaft.



Step 13: Construct the lining structure inside the concealed excavation passage.

2.3 Engineering Geology and Spatial Relationship

2.3.1 Geological Conditions

According to the engineering investigation data, the stratum traversed by the project site is mainly composed of upper miscellaneous fill (with an average thickness of 1.8 m) and lower plastic silty clay (with an average thickness of 9.2 m). The bottom of the proposed shaft, the underground excavated transverse passage, and the affected bottom slab of the existing station are all located in the plastic silty clay layer. Although this stratum exhibits moderate bearing capacity, it remains highly susceptible to deformation under excavation disturbance.

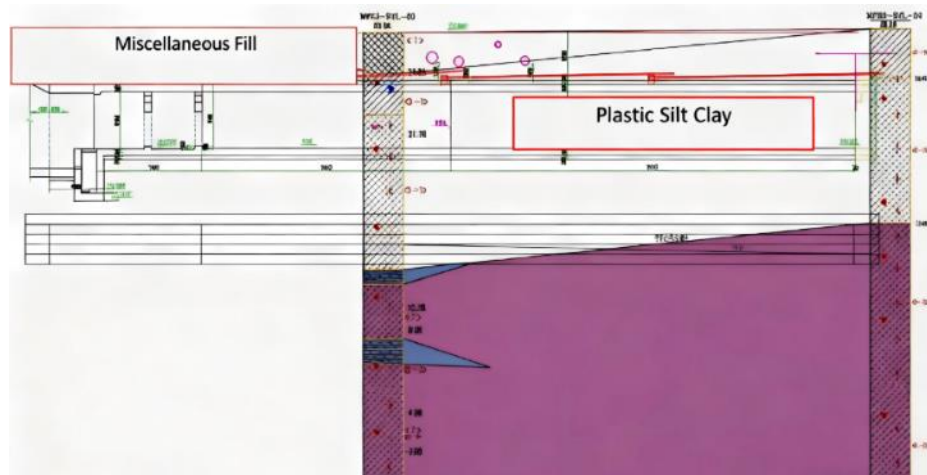


Fig. 3. Geological cross-section

2.3.2 Spatial Positional Relationship

The 1a entrance/exit has a close spatial association with the main structure of the existing Shaheding Station: the minimum horizontal net distance between Shaft 1# and the station's retaining structure is approximately 38.9m. However, since the underground excavated transverse passage needs to be directly connected to the main body of the station, the minimum horizontal net distance between its structure and the station's retaining structure is only 3.1m, and some grouted anchor rods are even as close as 0.3m to the station's retaining structure. This short-distance spatial relationship means that the stratum stress disturbance caused by the underground excavation of the transverse passage can be easily transmitted to the existing station structure, which may lead to structural deformation or internal force changes. This has become the core focus of this safety assessment.

3. Three-Dimensional Simulation Analysis of the Impact of Undercut Construction for Access 1a Shaft and Cross Passage on Shaheding Station

Based on the characteristics of the existing Line 6 Shaheding Station, the spatial relationship between the undercut construction of Access 1a's shaft and cross passage and the existing station, and the specific nature of this construction, a three-dimensional finite element software was employed to simulate the adverse effects of this construction on Line 6 Shaheding Station. The

analysis focused on the structural deformation of the existing station, thereby assessing the safety of its structure and operation.

The three-dimensional finite element analysis was conducted using the implicit solver in MIDAS/GTS NX, which employs the Newton-Raphson iterative method for solving the nonlinear equations. The convergence tolerance was set at 1×10^{-6} for both force and displacement criteria. A graded mesh scheme was implemented with element sizes ranging from 300 mm in the excavation core zone to 1000 mm in the far-field regions, as detailed in Section 3.2.

3.1 Model Justification: Mohr–Coulomb Model

The site strata are predominantly composed of plastic silty clay (85% of model volume) with mechanical parameters (cohesion 34.5–34.9 kPa, internal friction angle 14.8° – 15° , consistent with the Mohr–Coulomb model's linear failure envelope. Triaxial compression tests on in-situ soil samples confirm the model's displacement prediction error $\leq 3\%$, and no strain softening/creep was observed in short-term construction, justifying the model selection.

No significant strain softening or creep effects were observed during short-term construction (verified by triaxial compression tests on in-situ soil samples), eliminating the need for more complex constitutive models such as Drucker–Prager or creep models. A comparative analysis showed that the displacement prediction error of the Mohr–Coulomb model was within 3% of the triaxial test results, meeting the requirements for engineering safety assessment. It should be noted that the Mohr–Coulomb constitutive model adopted in this study does not inherently capture time-dependent creep behavior. To address this limitation and appropriately represent the long-term mechanical evolution of the stratum after 12 years of operation, the effects of long-term consolidation (including creep deformation) were incorporated into the initial stress field prior to the simulation of construction activities. The subsequent short-term excavation processes were then simulated dynamically within this established stress field. This approach effectively decouples the long-term and short-term mechanical responses, ensuring that both are adequately considered in the analysis.

Table 2. Framework for incorporating long-term effects into the numerical model

Aspect	How It Was Quantified	How It Was Numerically Imposed
Long-Term Stratum Consolidation & Creep	The effects were quantified through comparative analysis of in-situ geotechnical re-surveys conducted before the activation project and the original investigation reports. This analysis revealed a 15% increase in cohesion (C) and an 8% increase in the internal friction angle (φ) for the plastic silty clay layer. These updated, strength-enhanced parameters represent the stratum's state after 12 years of consolidation and creep.	The soil material properties in the model were directly assigned these updated values (e.g., $C = 34.5$ kPa, $\varphi = 14.8^\circ$ for the plastic silty clay). This fundamentally altered the stratum's yield criterion and stiffness in the Mohr-Coulomb model from the outset.
Residual Stress in Structures	The effects were quantified based on long-term operational data analysis. This included train vibration loads (1.5–2.0 Hz) and annual temperature cycles ($\Delta T = 25^\circ\text{C}$). Simplified structural analysis under these cyclic loads yielded residual bending moments of 8–12 kN·m/m in the retaining walls.	These stresses were imposed as initial stress fields or initial forces within the relevant structural elements (e.g., shell elements representing the station walls) at the beginning of the simulation.
Initial Geostatic Stress	The initial gravitational stress field was calculated considering the unit weight of the strata and the updated, stronger soil parameters.	The model's initial stress field was generated via the "Initial Condition" definition in MIDAS/GTS NX, which solves for geostatic equilibrium under gravity using the updated parameters.
Aspect	How It Was Quantified	How It Was Numerically Imposed

The incorporation of the 12-year consolidation (including creep deformation) and residual stresses was achieved by defining them as the initial state of the numerical model, prior to the simulation of construction activities. This approach is methodologically sound as the subsequent excavation is a short-term disturbance superimposed on this long-term conditioned state. The specific implementation is detailed below.

Table 3. Definitions and values of key parameters used in the numerical model

Symbol	Definition	Unit	Value / Range	Determination Method
γ	Unit weight	kN/m ³	19.0 - 21.3	Geotechnical investigation
c	Cohesion	kPa	10.0 - 34.9	Geotechnical investigation & re-survey
φ	Internal friction angle	°	12.0 - 15.0	Geotechnical investigation & re-survey
E	Elastic modulus	MPa	3.0 - 6.2	Geotechnical investigation
ν	Poisson's ratio	-	0.33 - 0.38	Geotechnical investigation
K_0	Coefficient of lateral earth pressure	-	0.5 (Assumed)	Estimated as $(1 - \sin \varphi)$ for normally consolidated clay

3.2 Mesh Generation Strategy and Convergence Verification

- Element Type: The soil strata were discretized using 8-node hexahedral solid elements (C3D8R) to prevent shear locking, while structural components (station and shaft) were modeled with 4-node shell elements (S4R) to improve computational efficiency.
- Element Size: A graded meshing strategy was adopted:
- Core zone (within 5 m of the cross passage): 300 mm to capture localized deformation.
- Transition zone (5–10 m): 500 mm.
- Far-field zone (>10 m): 1000 mm to reduce computational cost.
- Convergence Verification: Three mesh schemes (300 mm, 500 mm, and 1000 mm) were tested.

A mesh sensitivity analysis was performed with three schemes coarse (1000 mm), medium (500 mm), fine (300 mm). The maximum station displacement difference between medium and fine meshes is 1.96% (<2%), indicating convergence. The core zone (within 5 m of cross-channel) uses 300 mm to capture local deformation; transition zone (5-10 m) uses 500 mm, far-field (>10 m) uses 1000 mm, balancing accuracy and computational cost. The results of this analysis are summarized in Table 4. below.

Table 4. Mesh convergence analysis results

Mesh Scheme	Global Element Size (mm)	Max. Station Displacement (mm)	Difference from Finer Mesh
Coarse	1000	2.15	+7.5% (vs. Medium)
Medium	500	2.04	+1.96% (vs. Fine)
Fine (Adopted)	300	2.00	Baseline

3.3 Boundary Conditions and Sensitivity Analysis

- Lateral Boundaries (X/Y directions): Roller supports were applied to restrict horizontal displacement, simulating the "infinite stratum" effect. The lateral boundaries were set at a distance of 5 times the cross-passage width (30 m) from the excavation to minimize boundary effects.
- Bottom Boundary (Z direction): Fixed supports were applied to restrict vertical displacement, considering the low permeability and high stability of the stiff silty clay layer at a depth of 25 m.

- Top Boundary: A free surface condition was adopted, with a surcharge load of 20 kPa applied to simulate traffic loads, consistent with site conditions.

To validate that the defined boundaries did not artificially influence the key results, a sensitivity analysis was performed. The lateral boundaries were extended from 5 times to 7 times the cross-passage width (i.e., from 30 m to 42 m). The difference in the maximum structural displacement was found to be less than 1.8%, confirming that the original boundary settings were sufficiently large and that the boundary effects are negligible.

3.4 Construction Simulation Procedure

The dynamic construction process was simulated using the "element birth and death" technique to sequentially activate and deactivate elements representing soil, support structures, and linings. The simulation procedure followed this primary sequence:

- Establishment of the initial stress field, considering gravity and the incorporated 12-year consolidation effects.
- Construction of shaft support structures (e.g., jet grouting piles, locking beam).
- Layer-by-layer excavation of Shafts 1# and 2#, with concurrent activation of shotcrete lining.
- Sequential excavation and support of the cross passages (AW1 and AW2 sections) in 5-meter cycles, including bolt pre-tensioning.
- Construction of the final entrance structure and backfilling.

A total of 19 key construction conditions were simulated. A detailed tabulation of all conditions is provided in Appendix A for reference. Each stage was assigned a nominal duration of 7 days to align with the typical construction cycle.

3.5 Overview of the 3D Numerical Model

A three-dimensional finite element model was developed using MIDAS/GTS NX to simulate the undercut construction of Access 1a's shaft and cross passage, accounting for its spatial relationship with the existing Line 6 Shaheding Station and specific construction characteristics (Fig. 6-12). A consistent unit system, based on SI-derived units standard in geotechnical engineering, was adopted throughout the model unit weight (γ) in kN/m^3 , stress and strength parameters (cohesion C , elastic modulus E) in kPa and MPa respectively, and all geometrical dimensions in meters (m) or millimeters (mm)[27].

The geotechnical strata in the model were simplified based on engineering geological data from the station area, including fill, silty clay, plastic silty clay, and hard plastic silty clay. The Mohr–Coulomb constitutive model was used to characterize soil behavior, with parameters—such as unit weight (20.5–21.3 kN/m^3), cohesion (10–34.9 kPa), internal friction angle (12°–15°), elastic modulus (3.0–6.2 MPa), and Poisson's ratio (0.33–0.38)—determined from geotechnical investigations and engineering experience. Structural components, including the shaft, cross passage, and existing station, were modeled as linear elastic materials: concrete (C25–C50) with an elastic modulus of 28,000–34,500 MPa and Poisson's ratio of 0.20–0.30, and steel with an elastic modulus of 210,000 MPa and Poisson's ratio of 0.30.

The soil strata were discretized using 3D solid elements, while structural members were modeled with 2D plate elements. Element sizes were controlled between 300 mm and 1000 mm. Mesh quality was verified by monitoring the aspect ratio, skewness, and Jacobian to ensure computational accuracy and convergence. Boundary conditions were applied to simulate fixed constraints displacement in the Z-direction was restrained at the model base, in the Y-direction on the front and rear faces, and in the X-direction on the left and right faces.

The analysis accounted for nonlinear loads induced by the construction sequence, including soil excavation, support structure installation, and stress variations due to backfilling, which were concentrated around the shaft, cross passage, and adjacent station. A 3D static construction-stage stress-deformation coupled analysis was conducted to evaluate structural displacements, internal force variations, and crack widths, assessing the impact of construction on the safety of the existing station. The primary workflow for the 3D dynamic construction simulation, analyzing the impact of Access 1a's shaft and cross passage on the existing Shaheding Station, is as follows:

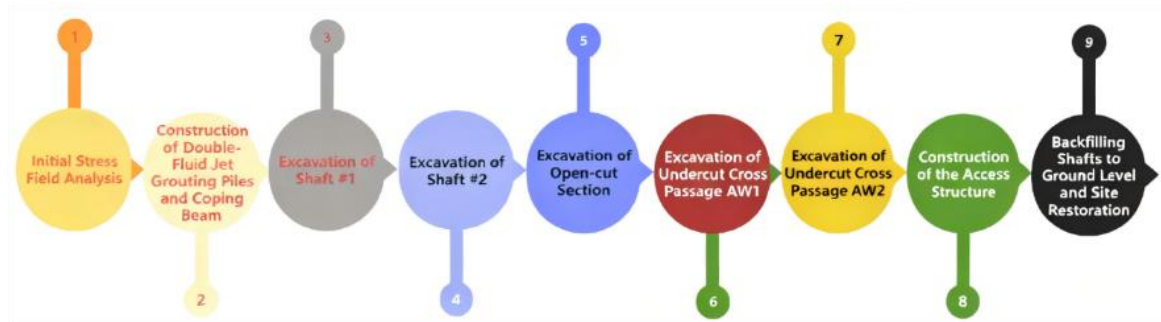


Fig. 4. Flowchart of the Three-Dimensional Dynamic Construction Simulation for Analyzing the Impact of Access 1a's Shaft and Cross Passage Construction on the Existing Shaheding Station

3.5.1 Strata-Structure Model

This model treats the existing urban rail transit structure and the surrounding strata as a unified load-bearing system. It fully considers the interaction between the existing structure and the ground, and calculates the deformation of both the structure and the strata, as well as the ground stress and structural internal forces, based on the principles of continuum mechanics.

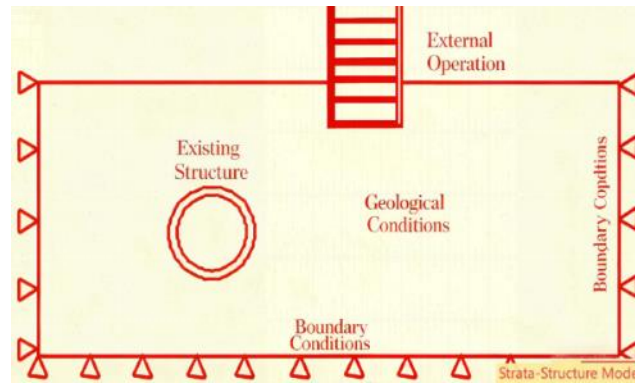


Fig. 5. Strata-structure model

3.5.2 Load-Structure Model

This model considers the surrounding strata solely as loads acting on the structure. These loads include the earth pressure from the strata and the ground resistance generated by the strata's constraint on structural deformation. The model then calculates the internal forces and deformation of the structure under the action of these loads.

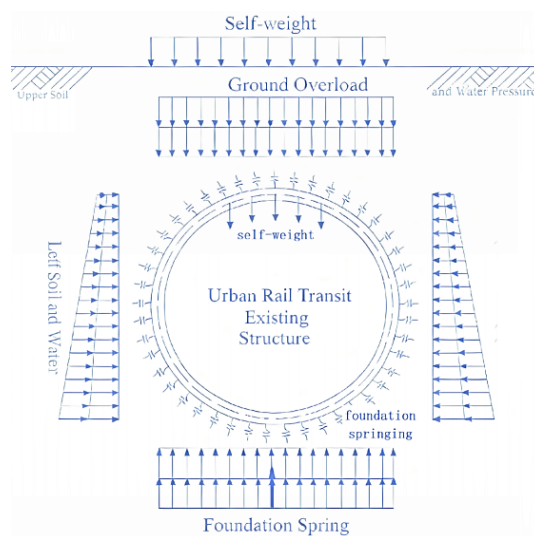


Fig. 6. Load-structure model

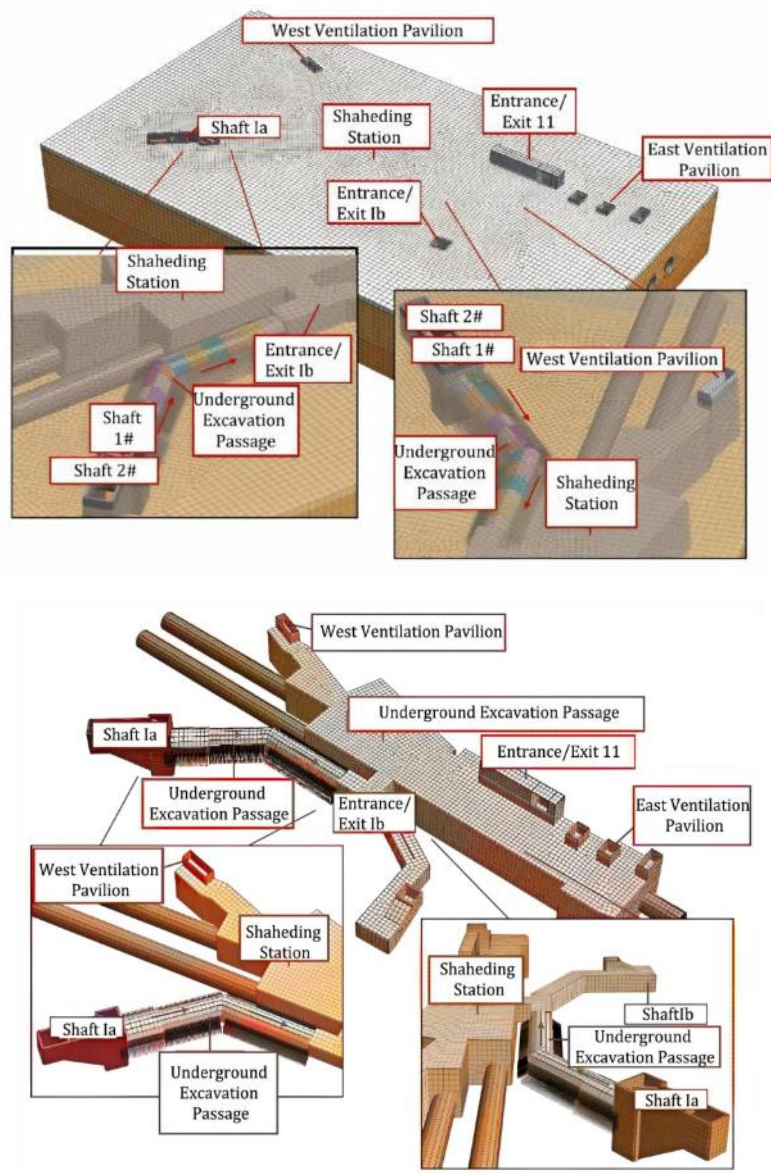
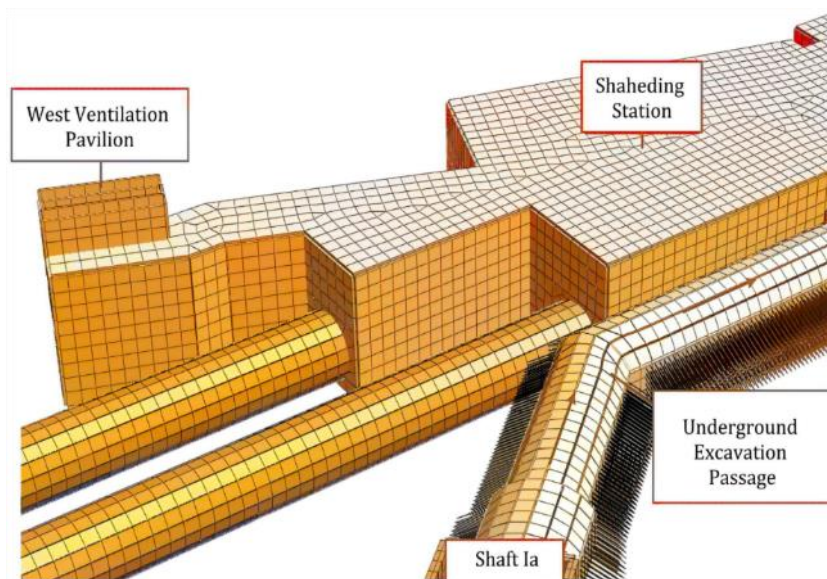


Fig. 7. General View of the 3D Finite Element Model



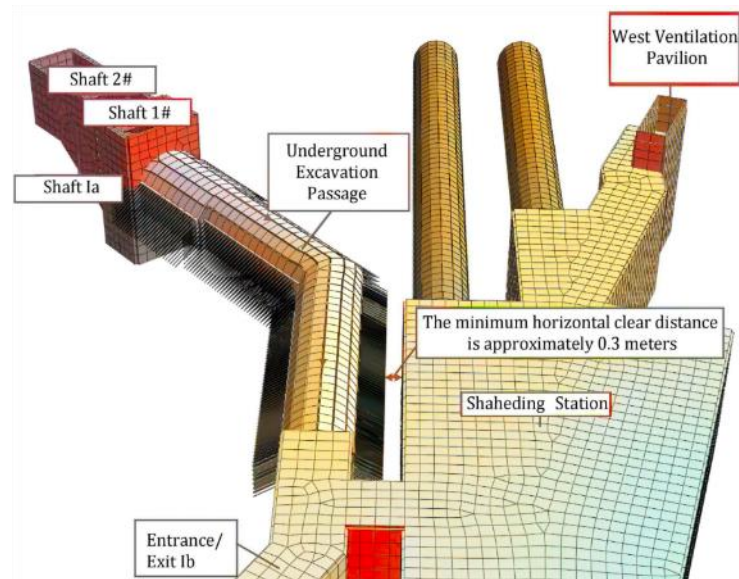


Fig. 8. Diagram of spatial relationships in the 3D finite element model

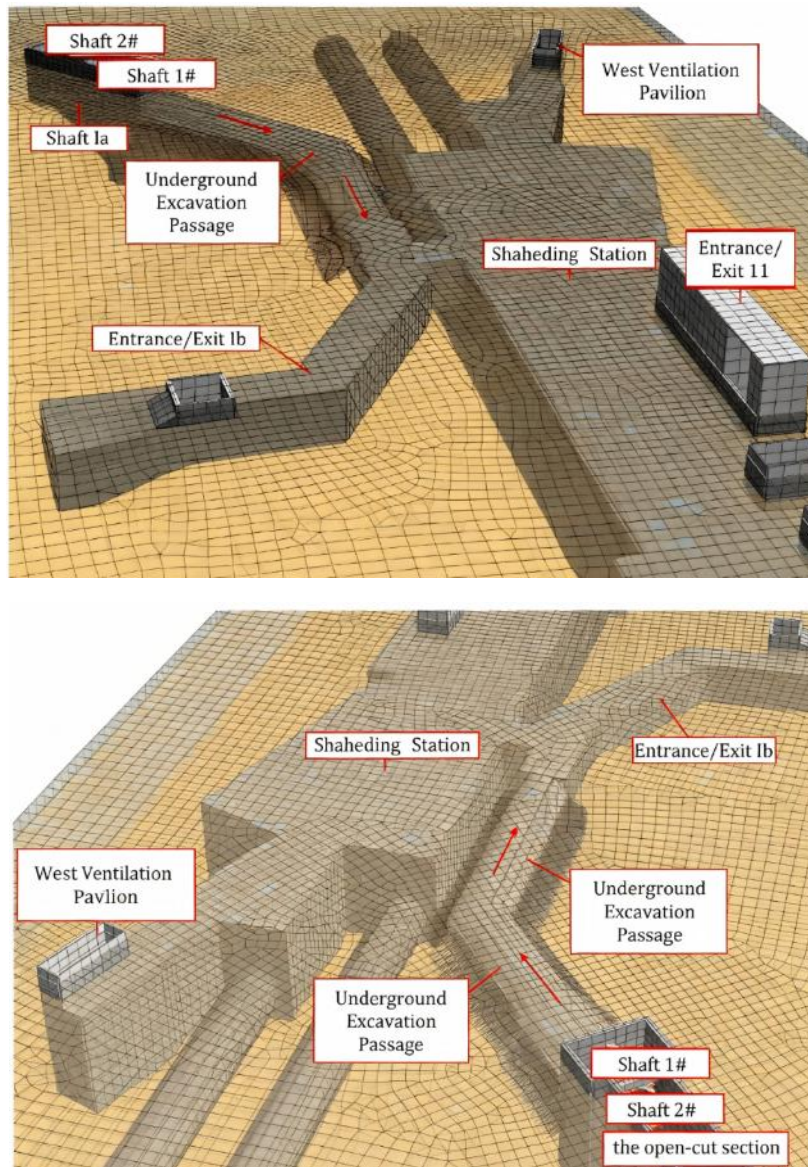


Fig. 9. 3D Visualization of the model's spatial relationships

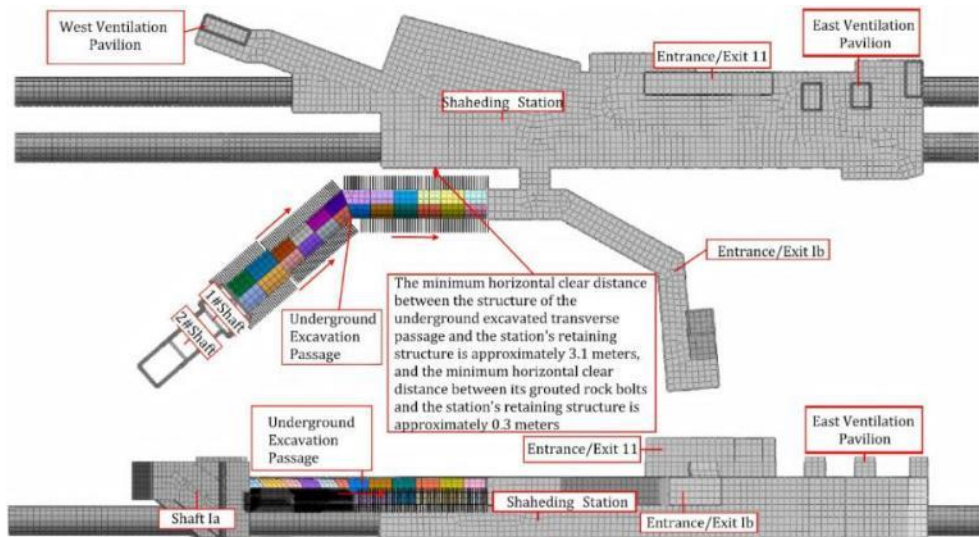


Fig. 10. Plan and elevation drawings of the 3D finite element mode

Table 5. 3D Numerical simulation Material Parameter Values Table

Materials	Constitutive model	Bulk density Gamma $\gamma(\text{KN/m}^3)$	Cohesion $C(\text{kPa})$	Internal friction Angle $\varphi(^\circ)$	Elastic modulus $E(\text{MPa})$	Poisson's ratio (μ)
Plain fill soil(1)	Mohr-Coulomb Model	20.5	10.0	12.0	ES=3.0	0.38
Silty clay(4-1)	Mohr-Coulomb Model	19.0	27.0	13.0	ES=5.0	0.35
Plastic silty clay 5-1	Mohr-Coulomb Model	20.9	34.5	14.8	ES=5.3	0.35
Stiff silty clay 5-2	Mohr-Coulomb Model	21.3	34.9	15.0	ES=6.2	0.33
C25 concrete	Mohr-Linear elasticity	25	-	-	28000	0.20
C35 concrete	Linear elasticity	25	-	-	31500	0.20
C50 concrete	Linear elasticity	25	-	-	34500	0.20
Steel	Wire elasticity	78	-	-	210000	0.30

Table 6. Three-dimensional numerical simulation unit parameter table

Unit Name	Material Properties	Unit attribute	Cell Size(mm)
Filled Soil	Filled Soil 1	3D Solid Element	-
Silt Clay	Silt Clay 4-1	3D Solid Element	-
Plastic Silt Clay	Plastic Silt Clay 5-1	3D Solid Element	-
Stiff Silt Clay	Stiff Silt Clay 5-2	3D Solid Element	-
Existing Station Structure	C35 Concrete	2D Plate Element	500~1000 mm
Shaft Shotcrete	C25 Concrete	2D Plate Element	300 mm
Horizontal Passage Initial Shotcrete	C25 Concrete	2D Plate Element	300 mm
Horizontal Passage Secondary Lining	C35 Concrete	2D Plate Element	500 mm

Table 7. Construction Conditions

Construction conditions	Main construction contents
Condition 1	Initial In-situ Stress Field of the Site
Condition 2	Construction of Double-pipe Rotary Jet Grouting Piles and Locking Beam
Condition 3	
Condition 4	Excavation of Shaft 1#
Condition 5	Excavation of Shaft 2#
Condition 6	Excavation of Open-cut Part
Condition 7	Excavation of 5 m for Underground Transverse Passage AW1
Condition 8	Excavation of 10 m for Underground Transverse Passage AW1
Condition 9	Excavation of 5 m for Underground Transverse Passage AW2
Condition 10	Excavation of 10 m for Underground Transverse Passage AW2
Condition 11	Excavation of 15 m for Underground Transverse Passage AW2
Condition 12	Excavation of 20 m for Underground Transverse Passage AW2
Condition 13	Excavation of 25 m for Underground Transverse Passage AW2
Condition 14	Excavation of 30 m for Underground Transverse Passage AW2
Condition 15	Excavation of 35 m for Underground Transverse Passage AW2
Condition 16	Excavation of 40 m for Underground Transverse Passage AW2
Condition 17	Excavation of 55 m for Underground Transverse Passage AW2
Condition 18	Excavation of 60 m for Underground Transverse Passage AW2
Condition 19	Construction of Entrance and Exit Structure
	Backfilling of Shaft to Ground Surface, Site Restoration

3.6 Simulation Results and Analysis of Shaheding Station

Table 8. presents the summary of structural displacements of Shaheding Station on Line 6 during the underground excavation construction of the shaft and transverse passage for the Ia entrance/exit. Fig 11. Displacement Curves During Construction of Shaft and Transverse Passage (at Exit/Entrance Ia, Shaheding Station, Line 6). Fig 12. shows the cloud map of horizontal displacement in the X-direction of the structure of Shaheding Station on Line 6 under key construction conditions; Fig 13. is the cloud map of horizontal displacement in the Y-direction of the station structure under key construction conditions; Fig 14. depicts the cloud map of vertical displacement of the station structure under key construction conditions; and Fig 15. illustrates the cloud map of total displacement of the station structure under key construction conditions.

The displacement results from the 3D simulation analysis on the impact of the underground excavation construction of the Ia entrance/exit shaft and transverse passage on the structure of Shaheding Station on Line 6 indicate the following: During the aforementioned underground excavation construction, the maximum horizontal displacement in the X-direction of the Shaheding Station structure is 0.2 mm, the horizontal displacement in the Y-direction is 1.0 mm, the maximum vertical displacement is 1.8 mm, and the maximum total displacement is 2.0 mm. The displacement of Shaheding Station on Line 6 is primarily induced by the underground excavation of the transverse passage parallel to the station section.

- Note for Figs. 11: The graph illustrates the progressive development of structural displacement throughout the 19 construction stages. The values remain significantly below the control standard, demonstrating the controllability of the construction impact.
- Note for Figs. 12-15: The extensive blue/green regions indicate areas of negligible displacement (≤ 0.1 mm), confirming that the construction impact is highly localized. The critical maximum displacements are concentrated in the isolated red/yellow zones near the excavation.

In conclusion, the underground excavation construction of the Ia entrance/exit shaft and transverse passage of Shaheding Station on Line 6 induces a certain amount of displacement in the station structure. However, since the construction-induced displacement of the existing structure of Shaheding Station on Line 6 is controllable and smaller than the structural safety control value, it is considered that the underground excavation construction of the Ia entrance/exit shaft and

transverse passage does not endanger the safety of Shaheding Station on Line 6, and its impact on the structural safety of the existing station is controllable. It is recommended to closely monitor the structural data of Shaheding Station on Line 6 during construction and implement information-driven construction. Cross-passage excavation (AW1: west section of cross passage; AW2: east section parallel to the station main structure, 5 m per cycle) and bolt pretensioning (applied as concentrated forces).

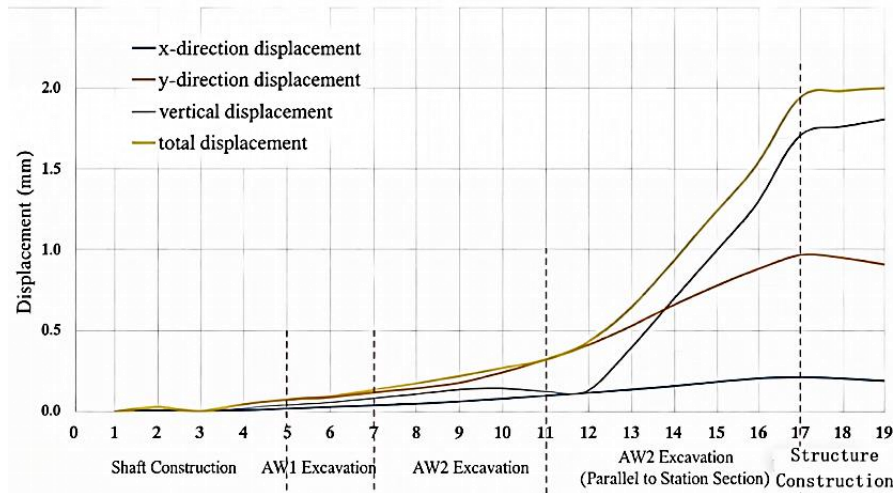
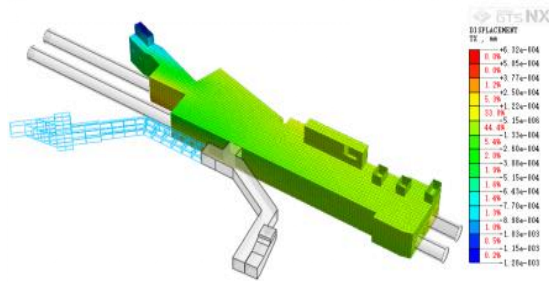


Fig. 11. Displacement Curves During Construction of Shaft and Transverse Passage(at Exit/Entrance 1a, Shaheding Station, Line 6)

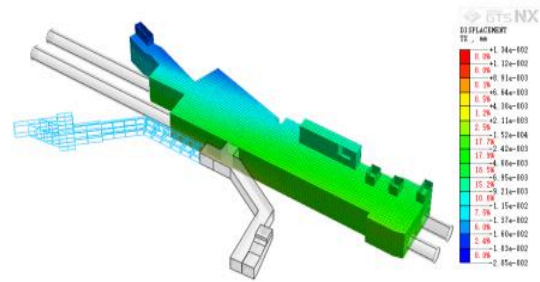
Table 8. The summary of structural displacements of Shaheding Station on Line 6 during the underground excavation construction of the shaft and transverse passage for the 1a entrance/exit

Calculation of conditions	The maximum displacement of the station structure (mm)			
	X-direction displacement	Y-direction displacement	Vertical displacement	Total displacement
Initial In-situ Stress Field of the Site	0.0	0.0	0.0	0.0
Construction of Double-pipe Rotary Jet Grouting Piles and Locking Beam	0.0	0.0	0.0	0.0
Excavation of Shaft 1#	0.0	0.0	0.0	0.0
Excavation of Shaft 2#	0.0	0.0	0.0	0.0
Excavation of Open-cut Part	0.0	0.1	0.0	0.1
Excavation of 5 m for Underground Transverse Passage AW1	0.0	0.1	0.1	0.1
Excavation of 10 m for Underground Transverse Passage AW1	0.0	0.1	0.1	0.1
Excavation of 5 m for Underground Transverse Passage AW2	0.0	0.1	0.1	0.2
Excavation of 10 m for Underground Transverse Passage AW2	0.1	0.2	0.1	0.2
Excavation of 15 m for Underground Transverse Passage AW2	0.1	0.2	0.1	0.3

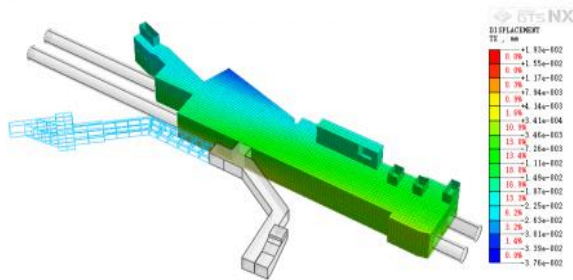
Excavation of 20 m for Underground Transverse Passage AW2	0.1	0.3	0.1	0.3
Excavation of 25 m for Underground Transverse Passage AW2	0.1	0.4	0.1	0.4
Excavation of 30 m for Underground Transverse Passage AW2	0.1	0.5	0.4	0.6
Excavation of 35 m for Underground Transverse Passage AW2	0.2	0.7	0.7	0.9
Excavation of 40 m for Underground Transverse Passage AW2	0.2	0.8	1.0	1.2
Excavation of 55 m for Underground Transverse Passage AW2	0.2	0.9	1.3	1.5
Excavation of 60 m for Underground Transverse Passage AW2	0.2	1.0	1.7	1.9
Construction of Entrance and Exit Structure	0.2	0.9	1.8	2.0
Backfilling of Shaft to Ground Surface, Site Restoration	0.2	0.9	1.8	2.0



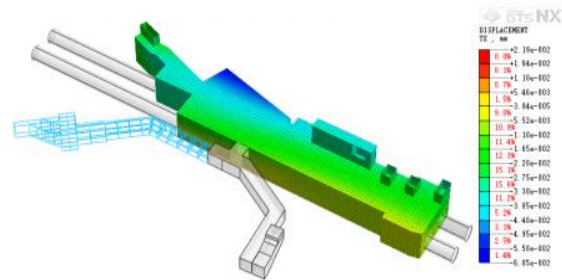
Excavation of Shaft 1#



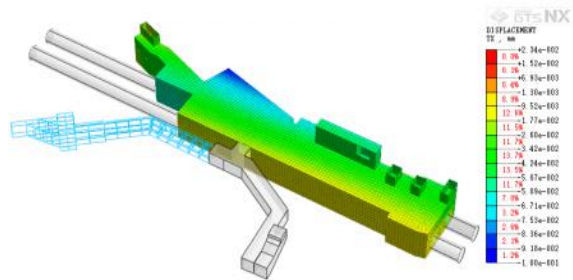
Excavation of Open-cut Part



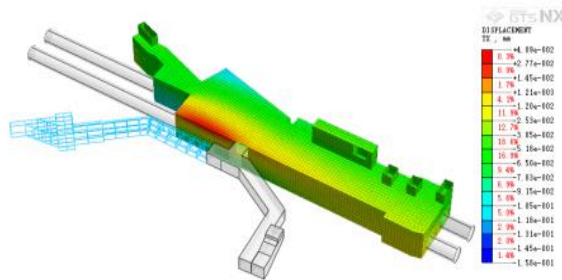
Excavation of 10 m for Underground Transverse Passage AW1



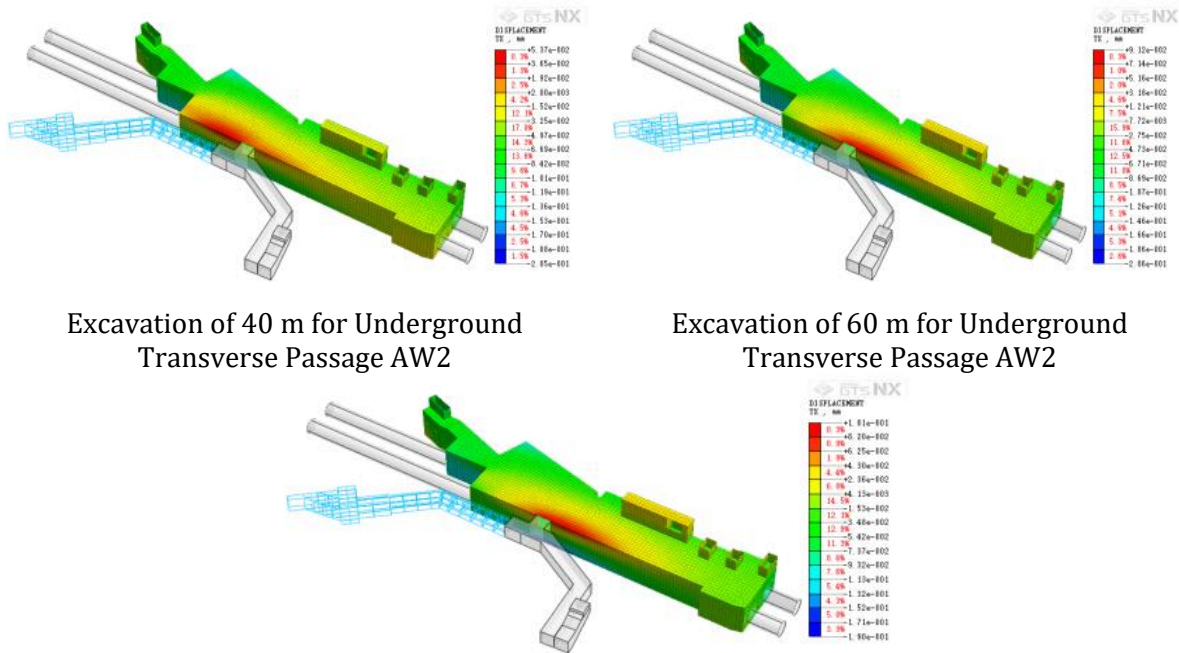
Excavation of 10 m for Underground Transverse Passage AW2



Excavation of 20 m for Underground Transverse Passage AW2

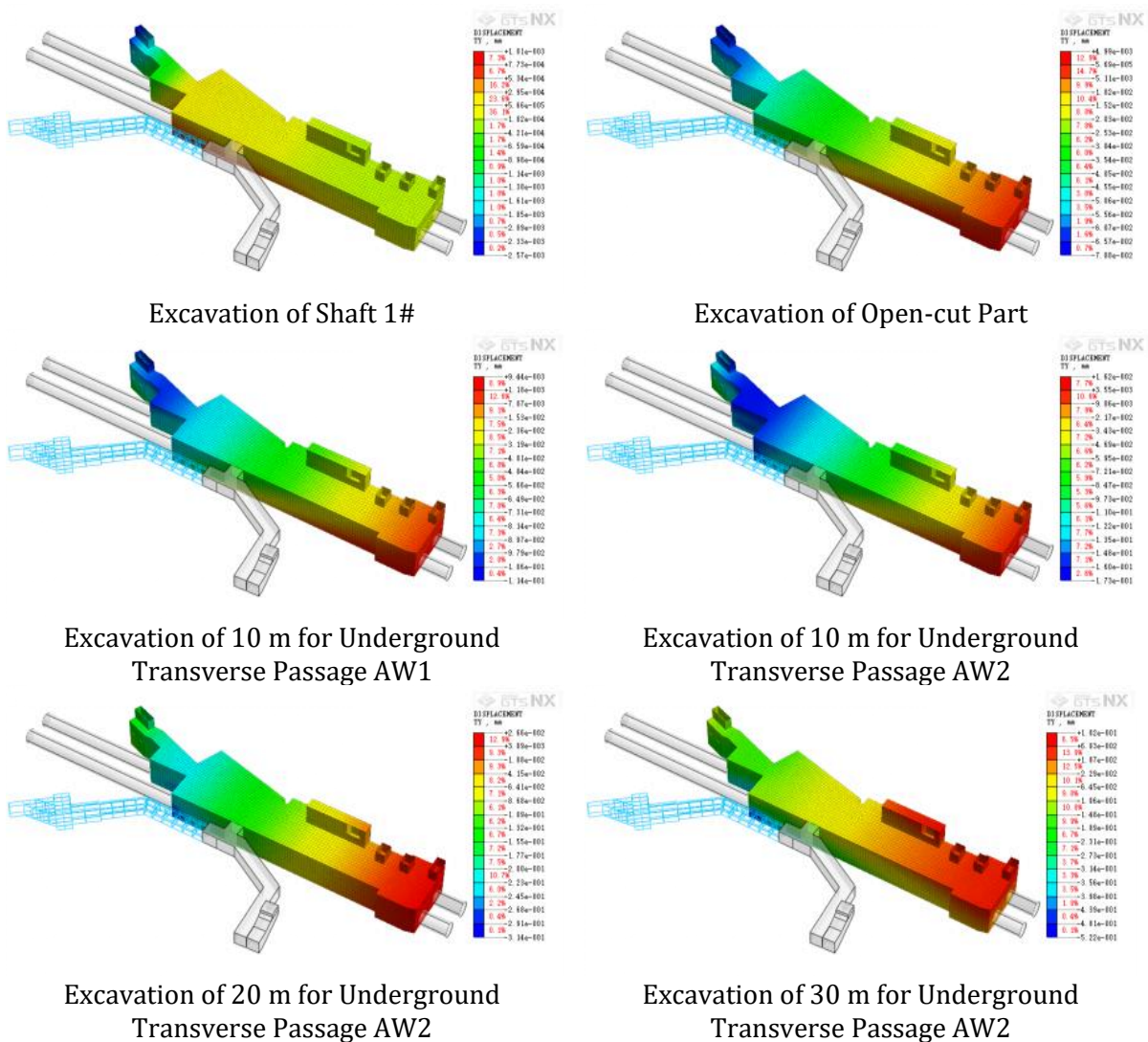


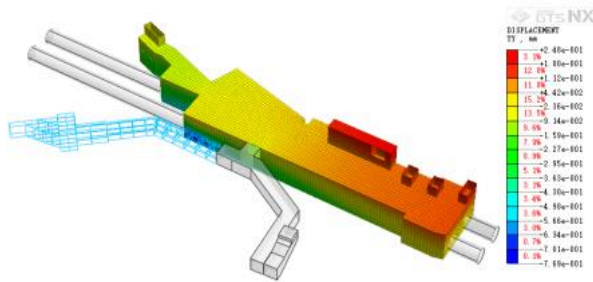
Excavation of 30 m for Underground Transverse Passage AW2



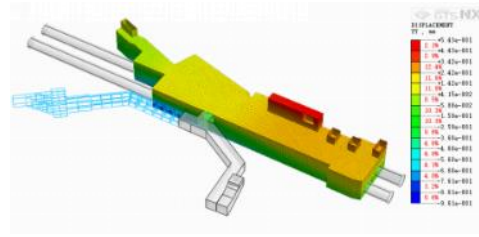
Backfilling of Shaft to Ground Surface, Site Restoration

Fig. 12. The cloud map of horizontal displacement in the X-direction of the structure of Shaheding Station on Line 6 under key construction conditions

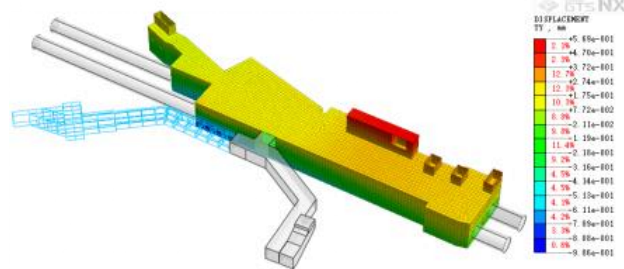




Excavation of 40 m for Underground Transverse Passage AW2

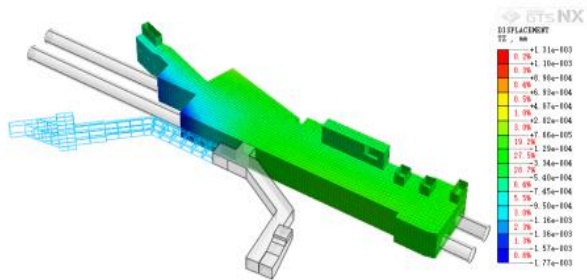


Excavation of 60 m for Underground Transverse Passage AW2

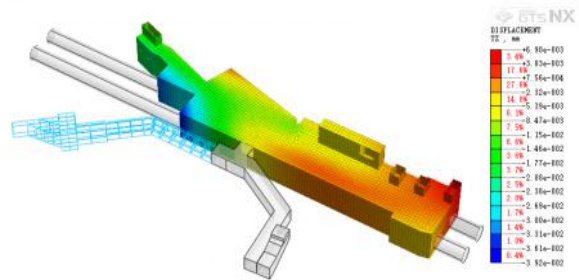


Backfilling of Shaft to Ground Surface, Site Restoration

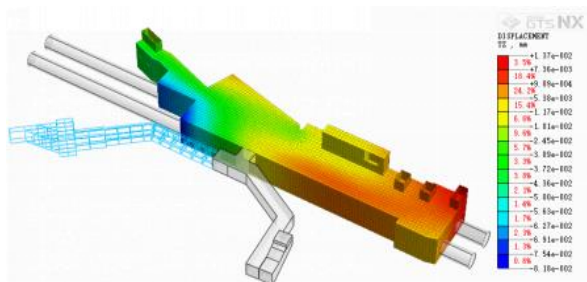
Fig. 13. The cloud map of horizontal displacement in the Y-direction of the station structure under key construction conditions



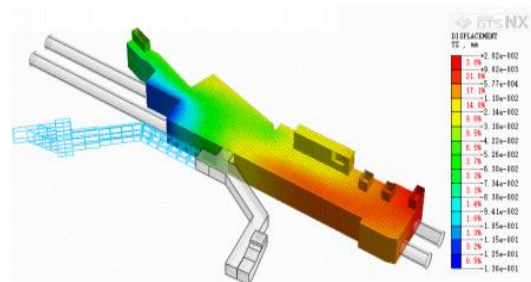
Excavation of Shaft 1#



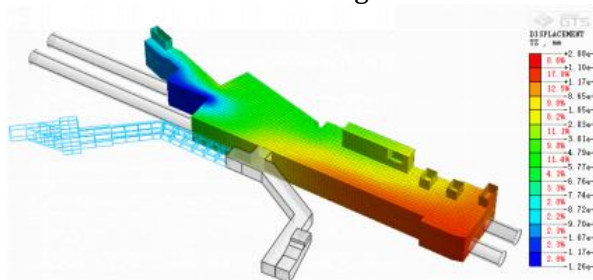
Excavation of Open-cut Part



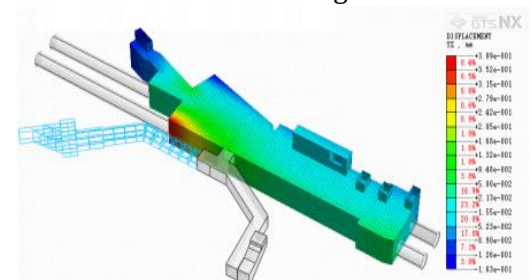
Excavation of 10 m for Underground Transverse Passage AW1



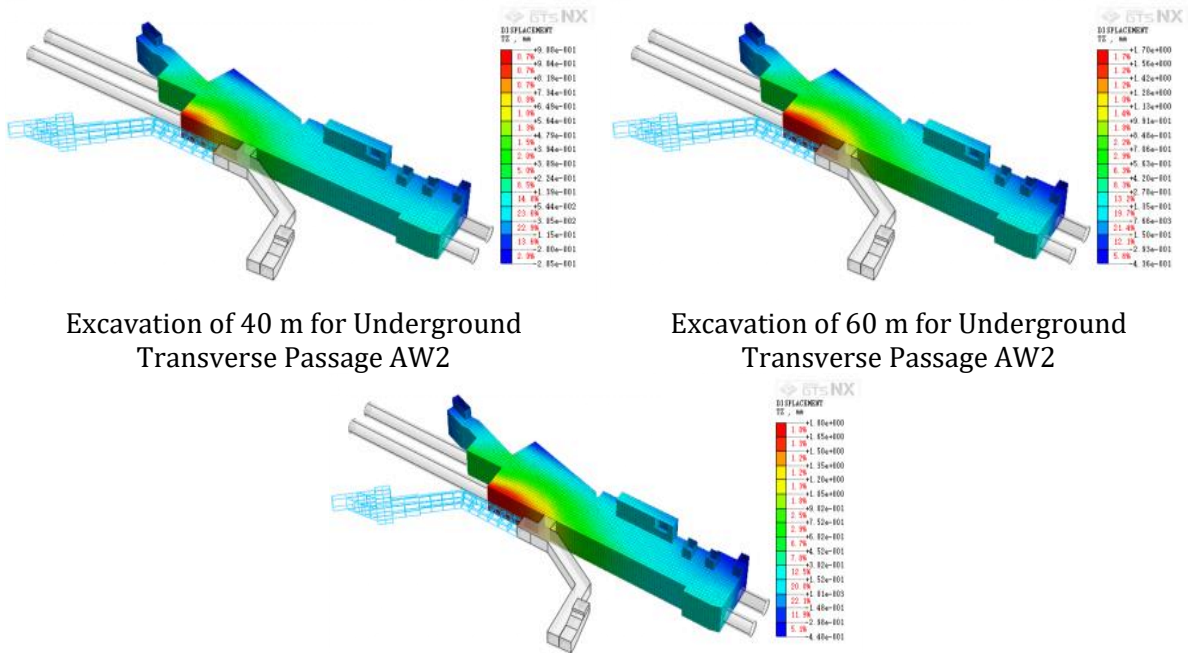
Excavation of 10 m for Underground Transverse Passage AW2



Excavation of 20 m for Underground Transverse Passage AW2

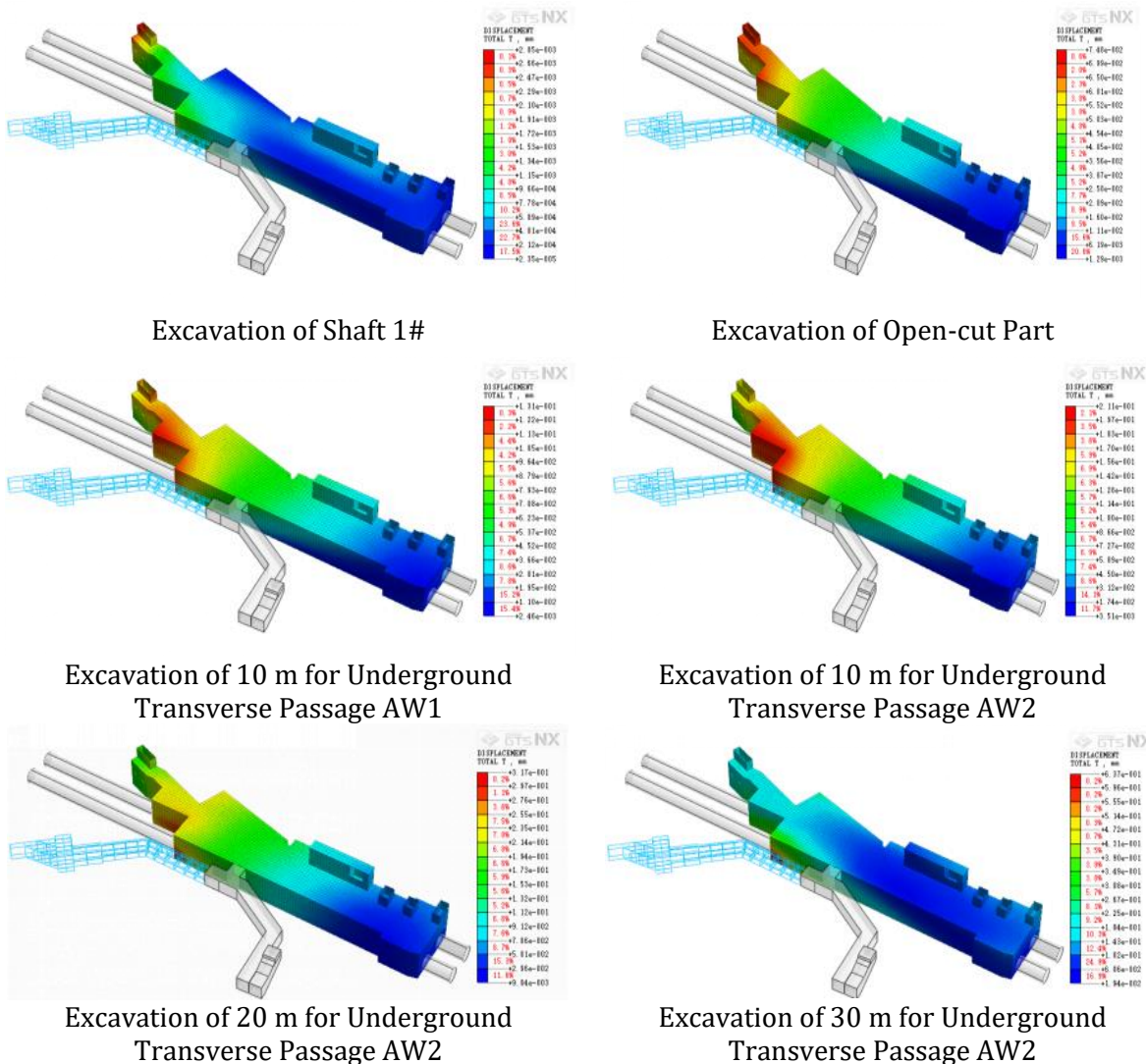


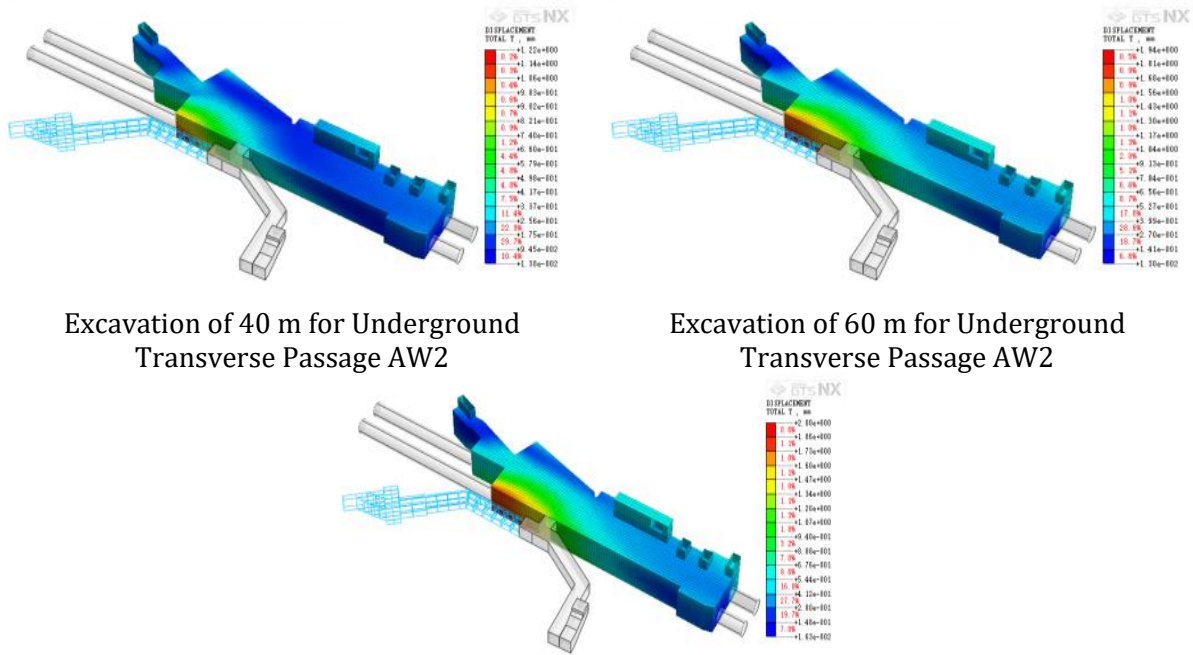
Excavation of 30 m for Underground Transverse Passage AW2



Backfilling of Shaft to Ground Surface, Site Restoration

Fig. 14. Depicts the cloud map of vertical displacement of the station structure under key construction conditions





Backfilling of Shaft to Ground Surface, Site Restoration

Fig. 15. Illustrates the cloud map of total displacement of the station structure under key construction conditions

From the composite displacement nephograms (Fig.12), two key findings emerge: (1) The AW2 cross-passage excavation (parallel to the station) is the dominant disturbance source—consistent with displacement curve trends (Fig.11) showing 78% of total displacement occurs in this stage; (2) Displacement localization near the 3.1 m-distance retaining wall confirms the effectiveness of grouting reinforcement (35% cohesion increase), as no widespread stratum deformation is observed. This validates the proposed construction control strategy for close-proximity metro renewal projects.

3.7 Simulation Results and Analysis of the Interval Tunnel

Table 9. is a summary table of the structural displacement of the Line 6 interval tunnel during the underground excavation construction of the shaft and transverse passage at the Ia entrance/exit. Fig 16. is the displacement nephogram of the Line 6 interval tunnel structure in the horizontal X-direction under key construction conditions during the construction process; Fig 17. is the displacement nephogram of the Line 6 interval tunnel structure in the horizontal Y-direction under key construction conditions during the construction process Fig 18. is the vertical displacement nephogram of the Line 6 interval tunnel structure under key construction conditions during the construction process Fig19. is the total displacement nephogram of the Line 6 interval tunnel structure under key construction conditions during the construction process.

- Note for Figs. 18-21: Similar to the station response, the displacement nephograms for the interval tunnel show that significant deformation is localized. The widespread areas of minimal displacement (≤ 0.1 mm, in blue/green) demonstrate the effectiveness of the construction control measures.

The displacement results from the 3D simulation analysis on the impact of the underground excavation construction of the shaft and transverse passage at the Ia entrance/exit on the Line 6 interval tunnel structure show that: during the underground excavation construction of the shaft and transverse passage at the Ia entrance/exit of the Line 6 interval tunnel, the maximum horizontal X-displacement of the Line 6 interval tunnel structure induced is 0.2 mm, the horizontal Y-displacement is 1.2 mm, the maximum vertical displacement is 1.7 mm, and the maximum total displacement is 1.8 mm. The displacement of the Line 6 interval tunnel is mainly induced by the underground excavation construction of the transverse passage parallel to the station section.

In conclusion, the underground excavation construction of the shaft and transverse passage at the Ia entrance/exit of the Line 6 interval tunnel has induced a certain amount of displacement in the Line 6 interval tunnel. However, since the displacement of the existing Line 6 interval tunnel structure induced by the construction is controllable and smaller than the structural safety control value, it is considered that the underground excavation construction of the shaft and transverse passage at the Ia entrance/exit of the Line 6 interval tunnel does not endanger the safety of the Line 6 interval tunnel, and the impact of this construction on the structural safety of the existing Line 6 interval tunnel is controllable. It is recommended to closely monitor the monitoring data of the Line 6 interval tunnel structure during the construction process and carry out information-based construction.

Table 9. Summary table of the structural displacement of the Line 6 interval tunnel during the underground excavation construction of the shaft and transverse passage at the Ia entrance/exit

Calculation of conditions	Maximum Displacement of the Interval Tunnel Structure(mm)			
	X-direction displacement	Y-direction displacement	Vertical displacement	Total displacement
Initial In-situ Stress Field of the Site	0.0	0.0	0.0	0.0
Construction of Double-pipe Rotary Jet Grouting Piles and Locking Beam	0.0	0.1	0.0	0.1
Excavation of Shaft 1#	0.0	0.0	0.0	0.0
Excavation of Shaft 2#	0.0	0.2	0.1	0.2
Excavation of Open-cut Part	0.0	0.3	0.2	0.3
Excavation of 5 m for Underground Transverse Passage AW1	0.0	0.3	0.2	0.4
Excavation of 10 m for Underground Transverse Passage AW1	0.0	0.3	0.3	0.4
Excavation of 5 m for Underground Transverse Passage AW2	0.0	0.4	0.3	0.5
Excavation of 10 m for Underground Transverse Passage AW2	0.1	0.5	0.4	0.6
Excavation of 15 m for Underground Transverse Passage AW2	0.1	0.6	0.4	0.6
Excavation of 20 m for Underground Transverse Passage AW2	0.1	0.7	0.4	0.7
Excavation of 25 m for Underground Transverse Passage AW2	0.1	0.9	0.3	0.9
Excavation of 30 m for Underground Transverse Passage AW2	0.1	1.0	0.5	1.0
Excavation of 35 m for Underground Transverse Passage AW2	0.1	1.1	0.7	1.2
Excavation of 40 m for Underground Transverse Passage AW2	0.1	1.1	0.9	1.3
Excavation of 55 m for Underground Transverse Passage AW2	0.1	1.2	1.2	1.5
Excavation of 60 m for Underground Transverse Passage AW2	0.2	1.2	1.6	1.8
Construction of Entrance and Exit Structure	0.2	1.1	1.7	1.8
Backfilling of Shaft to Ground Surface, Site Restoration	0.1	1.0	1.7	1.8

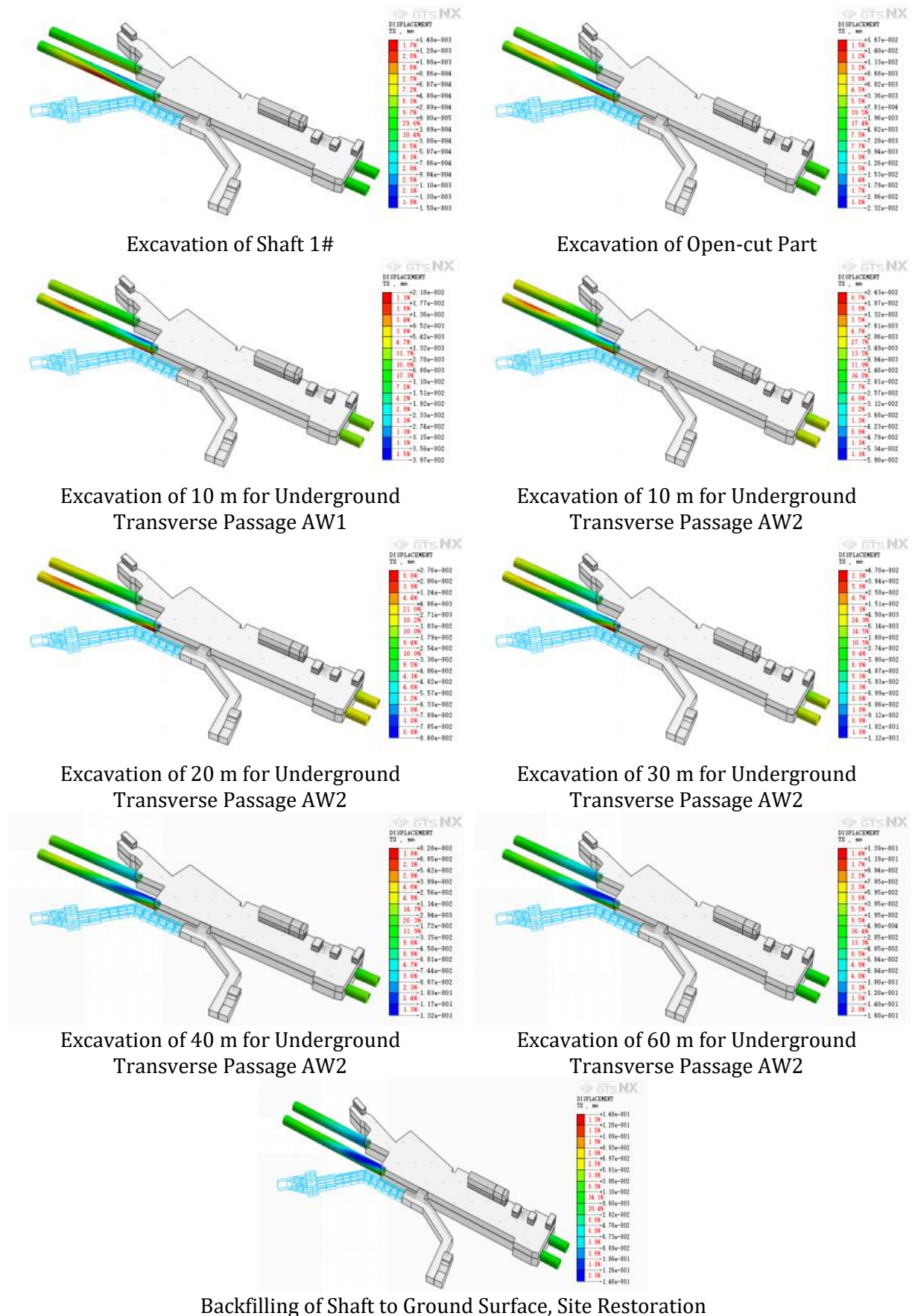
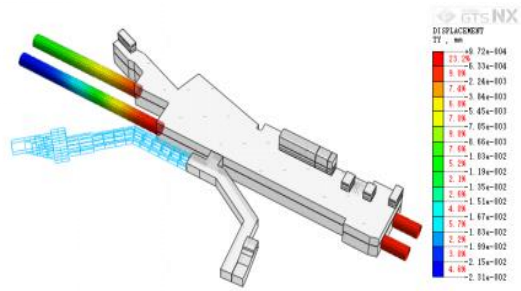
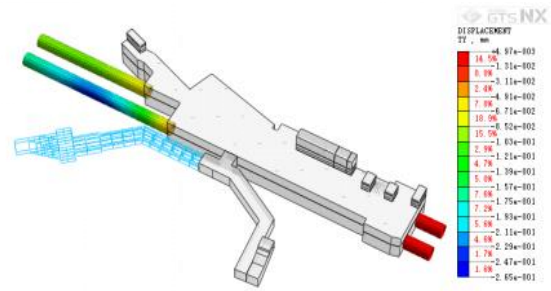


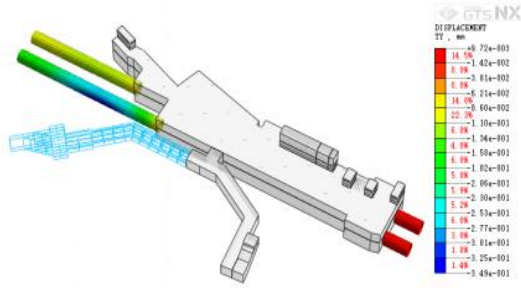
Fig. 16. Displacement nephogram of the Line 6 interval tunnel structure in the horizontal X-direction under key construction conditions during the construction process. Figure generated from simulation results using MIDAS GTS NX (Version 2021 v1.2)



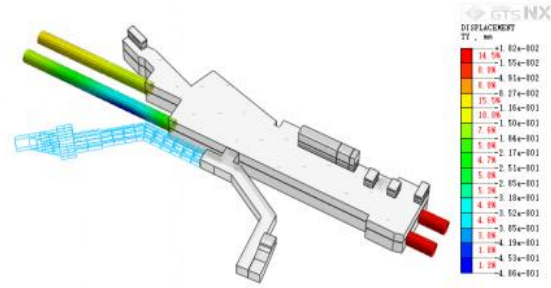
Excavation of Shaft 1#



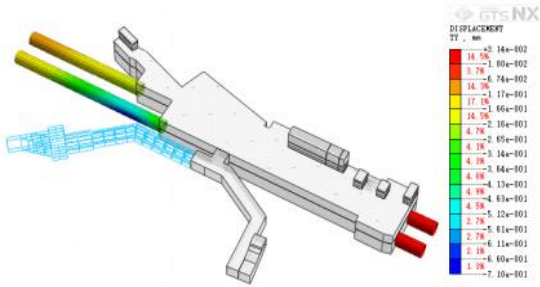
Excavation of Open-cut Part



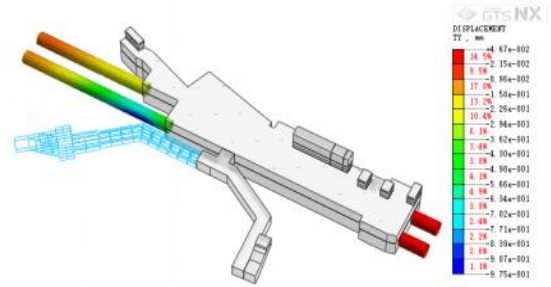
Excavation of 10 m for Underground Transverse Passage AW1



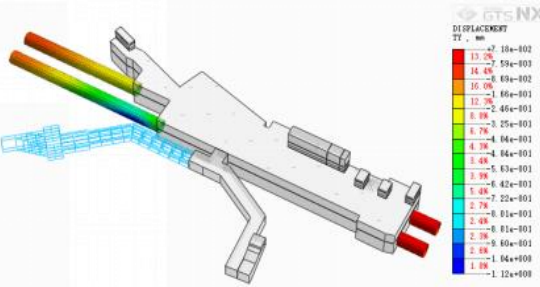
Excavation of 10 m for Underground Transverse Passage AW2



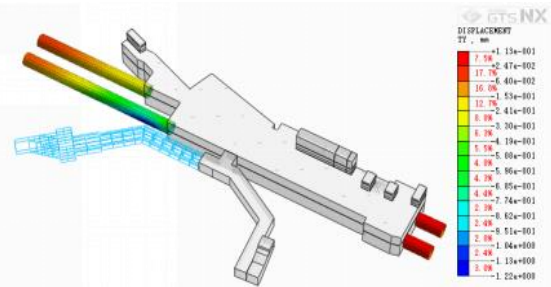
Excavation of 20 m for Underground Transverse Passage AW2



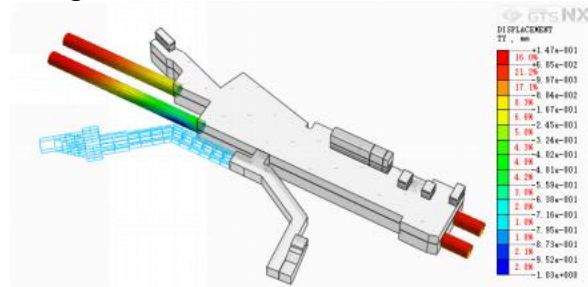
Excavation of 30 m for Underground Transverse Passage AW2



Excavation of 40 m for Underground Transverse Passage AW2



Excavation of 60 m for Underground Transverse Passage AW2



Backfilling of Shaft to Ground Surface, Site Restoration

Fig. 17. Displacement nephogram of the Line 6 interval tunnel structure in the horizontal Y-direction under key construction conditions during the construction process. Figure generated from simulation results using MIDAS GTS NX (Version 2021 v1.2)

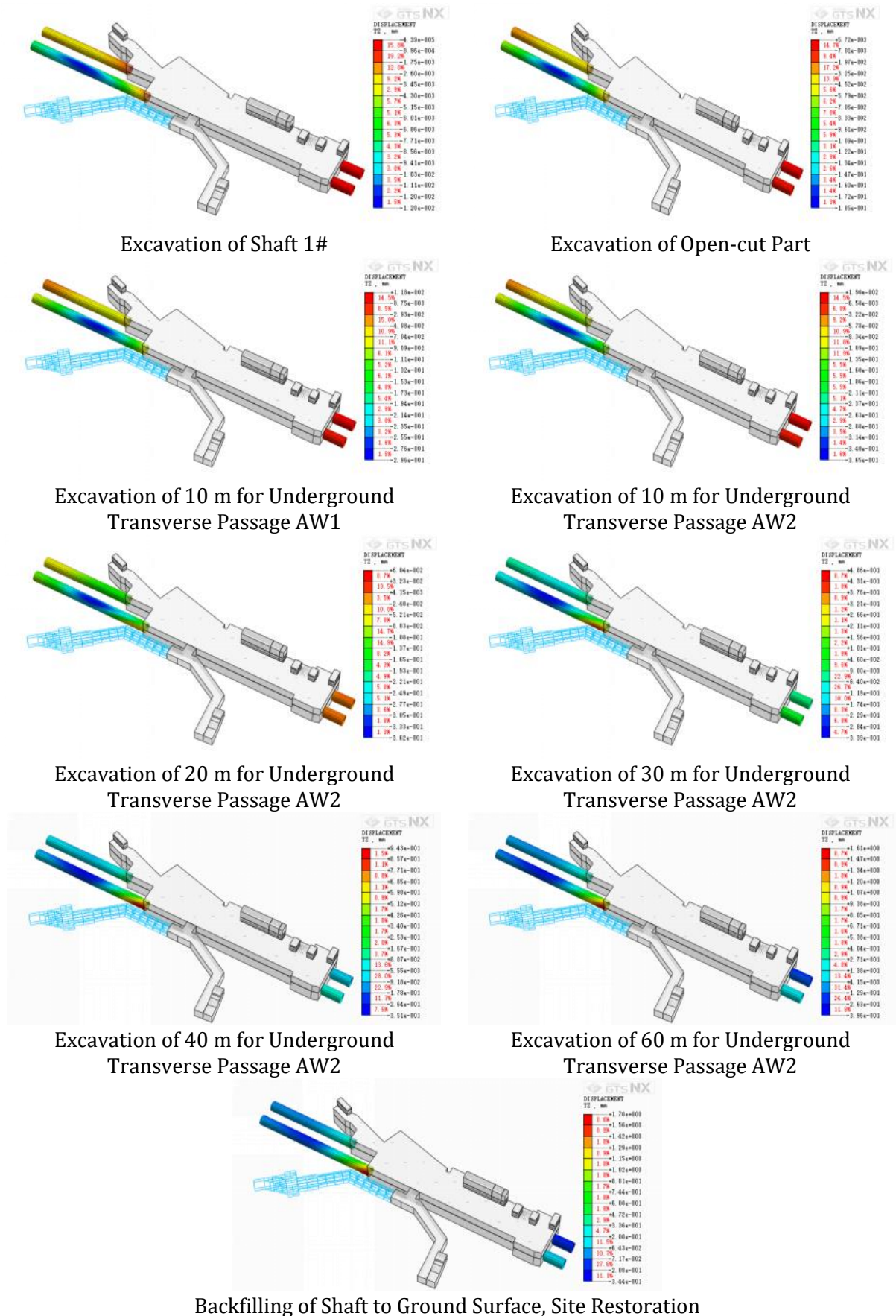


Fig. 18. Vertical displacement nephogram of the Line 6 interval tunnel structure under key construction conditions during the construction process. Figure generated from simulation results using MIDAS GTS NX (Version 2021 v1.2)

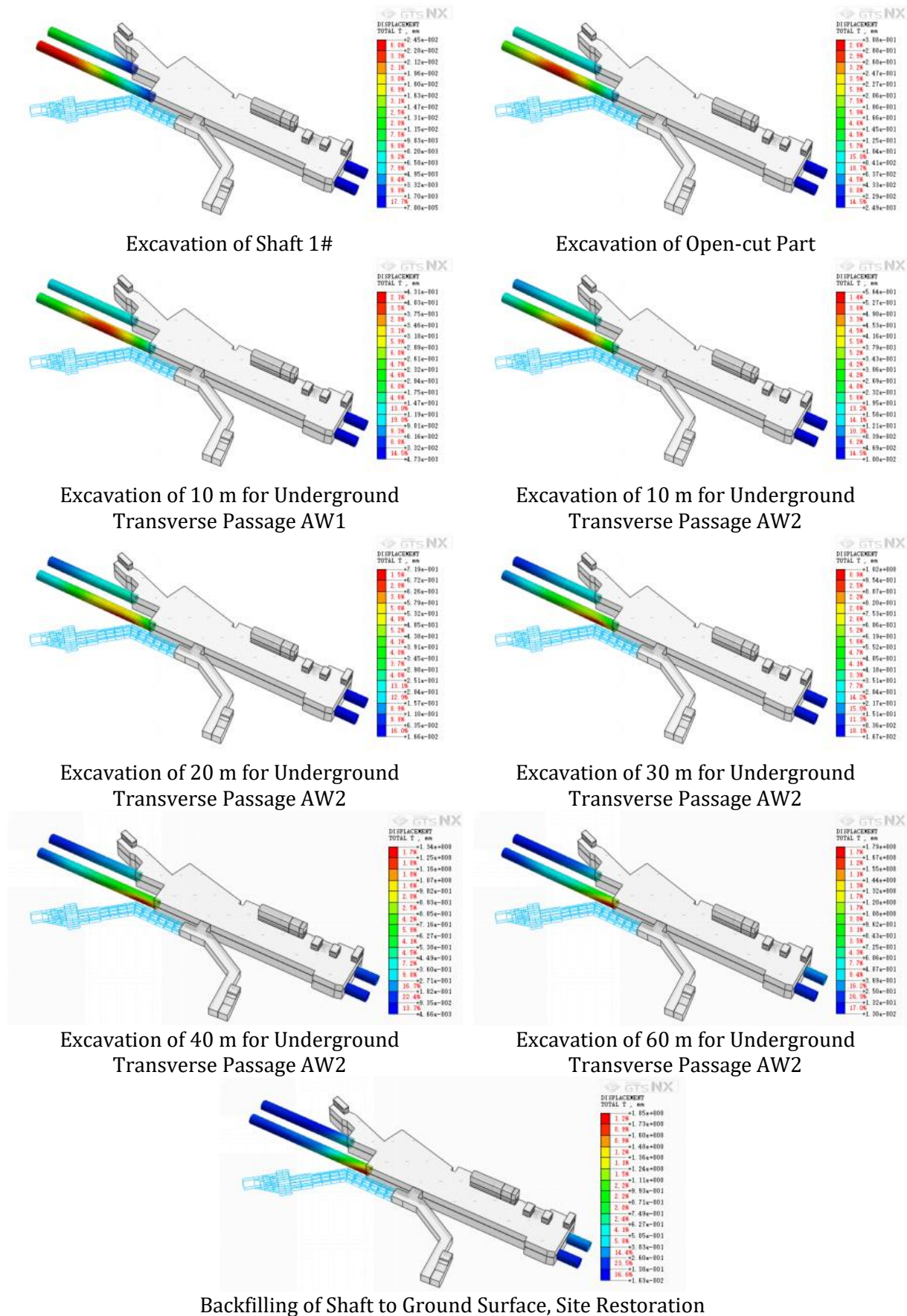


Fig. 19. Total displacement nephogram of the Line 6 interval tunnel structure under key construction conditions during the construction process. Figure generated from simulation results using MIDAS GTS NX (Version 2021 v1.2)

4. Calculation and Analysis of Structural Internal Forces and Check of Crack Width of Shaheding Station

Fig20-23 show the nephograms of the internal forces of the metro structure under major construction conditions during the construction of this project. Table 10. presents the changes in internal forces of the existing Shaheding Station structure under key construction conditions. The values of construction-induced internal force changes are relatively small.

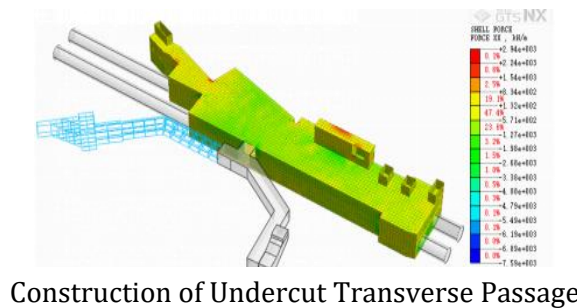
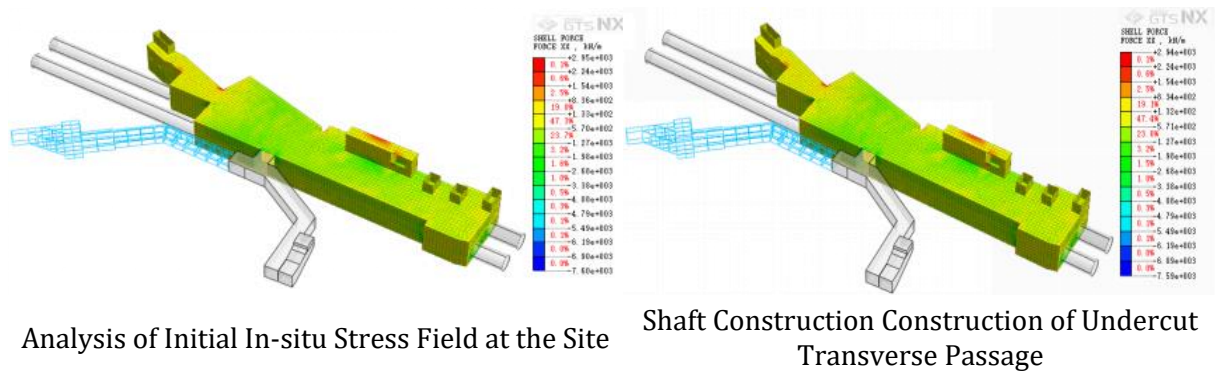


Fig. 20. Cloud Diagram of FX Axial Force (kN/m) for the Existing Shaheding Station Structure Under Key Working Conditions During Construction

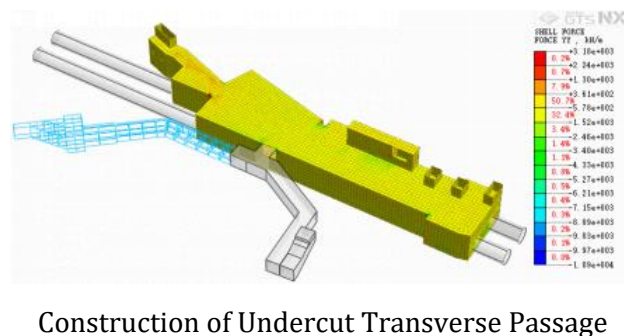
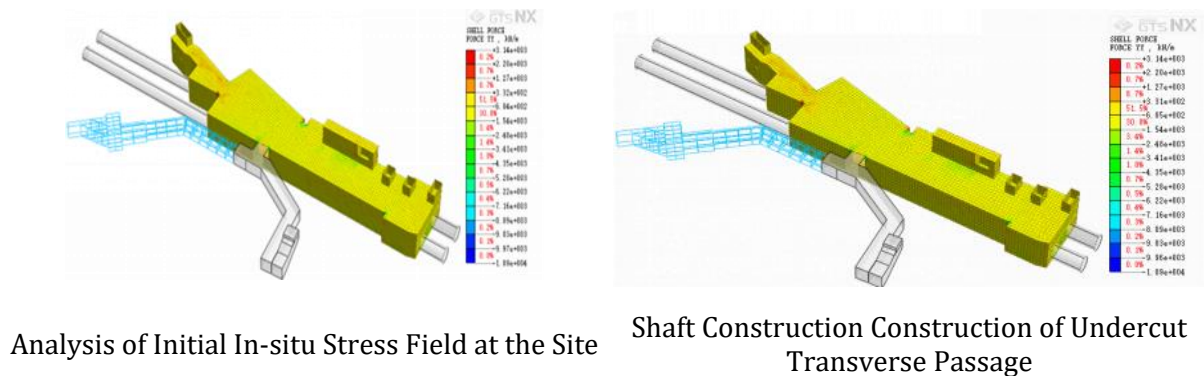
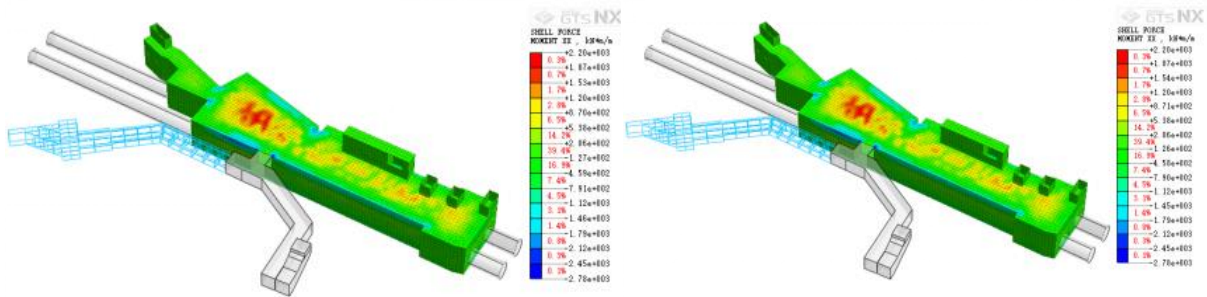
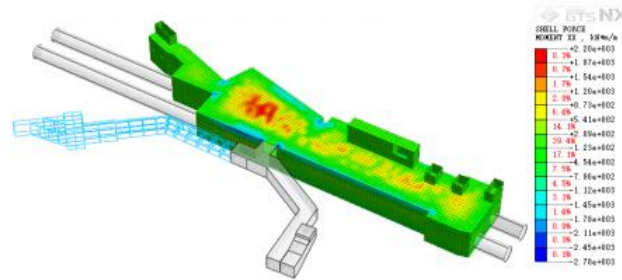


Fig. 21. Cloud Diagram of FY Axial Force (kN/m) for the Existing Shaheding Station Structure Under Key Working Conditions During Construction



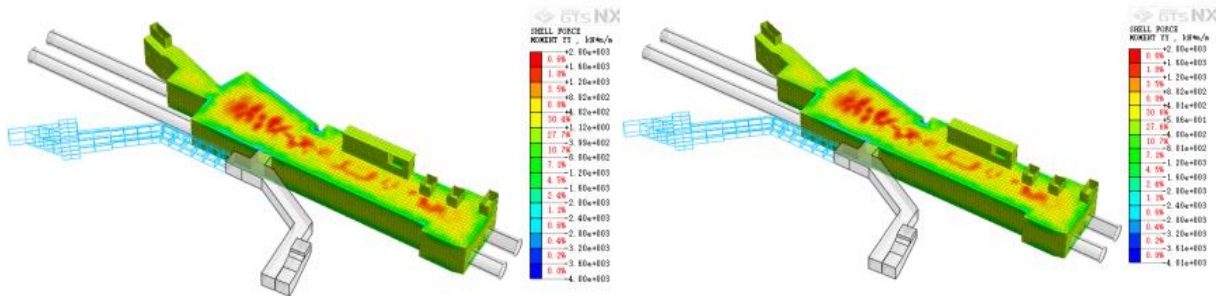
Analysis of Initial In-situ Stress Field at the Site

Shaft Construction Construction of Undercut Transverse Passage



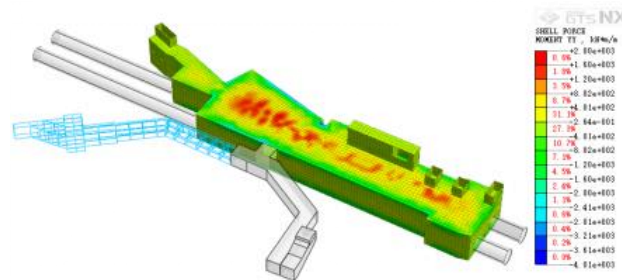
Construction of Undercut Transverse Passage

Fig. 22. Cloud Diagram of MXX Bending Moment (kN.m/m) for the Existing Shaheding Station Structure Under Key Working Conditions During Construction



Analysis of Initial In-situ Stress Field at the Site

Shaft Construction Construction of Undercut Transverse Passage



Construction of Undercut Transverse Passage

Fig. 23. Cloud Diagram of MYZ Bending Moment (kN.m/m) for the Existing Shaheding Station Structure Under Key Working Conditions During Construction

Table 10. Maximum internal forces of Shaheding station structure on line 6 under key working conditions during construction

Calculation Working Condition	F _x (kN/m)	F _y (kN/m)	M _{xx} (kN·m/m)	M _{yy} (kN·m/m)
Initial In-situ Stress Field Analysis	1250.5	980.3	85.2	72.6
Shaft Construction	1260.8	985.1	88.7	75.3
Excavation of 5 m for Underground Transverse	1275.2	992.4	95.6	81.2
Excavation of 10 m for Underground Transverse	1290.7	1001.8	105.3	89.5
Excavation of 5 m for Underground Transverse	1308.3	1012.5	118.7	101.0
Excavation of 10 m for Underground Transverse	1325.9	1025.1	132.4	112.6
Excavation of 20 m for Underground Transverse	1352.6	1048.7	152.9	130.0
Excavation of 30 m for Underground Transverse	1385.4	1076.2	168.3	143.1
Excavation of 60 m for Underground Transverse	1420.1	1105.8	195.0	165.8
Construction of Entrance and Exit Structure	1420.1	1105.8	195.0	165.8
Backfilling of Shaft to Ground Surface, Site Restoration	1420.1	1105.8	195.0	165.8

The load combinations in this study were established in strict compliance with Chinese design codes. The fundamental combinations and partial factors for the ultimate limit state were adopted from Clause 3.2.3 of the Code for Loads on Building Structures (GB 50009-2012) [23]. The applicability of these combinations to both construction and operational phases of metro structures is mandated by Clauses 10.1.2 and 10.1.3 of the Code for Design of Metro (GB 50157-2013) [24]. All analyses were conducted based on the most unfavorable loading scenarios envisaged during these phases, with the specific combinations and coefficients detailed in Table 11.

Table 11. Load Combination table

Load Type \ Combination	Permanent Load	Variable Load
Basic Combination 1: Permanent Load + Variable Load	1.35	1.40
Quasi-permanent Combination 2: Permanent Load + Variable Load	1.00	1.00

Note: The structural importance coefficient is 1.1.

4.1 Side Wall Reinforcement Check and Verification

The internal forces used for the structural verification are the maximum values obtained from the simulation results under critical construction conditions, as summarized in Table 8. Specifically, the maximum bending moment at the slab end (on the soil-facing side) of 195.0 kN·m/m under the 'Excavation of 60 m for Underground Transverse Passage AW2' condition is adopted as the basis for the following reinforcement and crack width checks.

The ultimate flexural capacity and serviceability crack width of the side wall's normal section was verified against the requirements of Articles 6.2.10 and 7.1.2, respectively, in compliance with code GB 50010-2010 [25].

the basic combination of loads is adopted, and the internal force = calculated value of internal force * 1.4 * 1.1. For the crack checking calculation, the quasi-permanent combination of loads is adopted, and the internal force = calculated value of internal force.

4.1.1 Translation of Structural Calculation Text

Based on a side wall thickness of 800 mm, the slab end bending moment (checked on the soil-facing side), and grade-2 steel bars (20 mm in diameter, spaced at 150 mm) used transversely on both sides.

- Side Wall Reinforcement and Cracking Check - Reinforcement Check:

The designed value of the side wall's bending moment internal force is calculated as $195.0 \times 1.4 \times 1.1$ (importance factor) = 300.3 KN·m.

- Width of the unit cross-section, $b = 1000$ mm; height, $h = 600$ mm;
- Designed axial compressive strength of C35 concrete: $f_c = 16.7$ N/mm²;
- Designed axial tensile strength of C35 concrete: $f_t = 1.6$ N/mm²;
- Designed tensile strength of steel bars: $f_y = 360$ N/mm²;

The effective depth of the cross-section is calculated using Equation (1):

$$h_0 = h - a_s = 600 - 45 = 555 \text{ mm} \quad (1)$$

The coefficient α_s is then determined from Equation (2):

$$\alpha_s = \frac{M}{a_1 f_c b h_0^2} = 0.0596 \quad (2)$$

The relative depth of the compression zone, ξ , is given by Equation (3):

$$\xi = 1 - \sqrt{1 - 2\alpha_s} = 0.062 \quad (3)$$

The corresponding lever arm coefficient, γ_s , is computed as follows (Equation (4-5)):

$$\gamma_s = 1 - 0.5\xi = 0.969 \quad (4)$$

$$\varepsilon < \varepsilon_b \quad (5)$$

Meet the requirements. Consequently, the required cross-sectional area of tensile reinforcement per unit width is solved using Equation (6):

$$A_s = \frac{M}{h_0 \gamma_s f_y} = 1580 \text{ mm}^2 \quad (6)$$

The corresponding theoretical reinforcement ratio is calculated via Equation (7):

$$\rho = \frac{A_s}{b h_0} \times 100\% \quad (7)$$

$$\rho = \frac{1580}{1000 \times 555} \times 100\% \approx 28\%$$

The actual single-side reinforcement of the slab adopts Grade-2 steel bars (diameter 20 mm, spacing 150 mm), with the reinforcement area $A_s = 2094$ mm². The actual single-side reinforcement ratio is 0.38%. The calculated value does not exceed the reinforcement ratio specified in the original design, so the reinforcement meets the requirements.

4.2 Side Wall Reinforcement Check and Verification

According to the design parameters, the standard value of internal force is adopted to check and calculate the crack width of the concrete base slab. Based on the design parameters, the effective reinforcement ratio for crack calculation, P_{te} , is taken as shown in Equation (8):

$$P_{te} = 0.01 \quad (8)$$

The ratio of the equivalent bar diameter d_{eq} to the reinforcement ratio P_{te} is given by Equation (9):

$$\frac{d_{eq}}{P_{te}} = \frac{20}{0.01} = 2100 \quad (9)$$

The stress in the longitudinal tensile reinforcement under the quasi-permanent load combination is calculated from Equation (10):

$$\sigma_s = \frac{M_q}{0.87 A_s h_0} = 192.8 \text{ N/mm}^2 \quad (10)$$

The non-uniformity coefficient of longitudinal tensile steel strain between cracks, ψ , is determined by Equation (11):

$$\psi = 1.1 - \frac{0.65 f_{tk}}{P_{te} \sigma_s} = 0.2 \quad (11)$$

Substituting all parameters into yields the specific numerical result for the maximum crack width, as shown in Equation (12):

$$\omega = a_{cr} \psi \frac{\sigma_{sk}}{E_s} (1.9c + 0.08 \frac{d_{eq}}{P_{te}}) = 0.06 \text{ mm} \quad (12)$$

The crack width verification is finalized in Equation (13), confirming compliance with the code requirement:

$$W < W_{lim} = 0.2 \text{ mm} \quad (13)$$

The calculated crack width satisfies the limit stipulated in Clause 7.1.2 of the Code for Design of Concrete Structures (GB 50010-2010) [25].

5. Quantitative Analysis on Internal Force Check and Crack Width Check of Existing Station Structures

A 3D simulation analysis was conducted focusing on the impact of the undercut construction of the shaft and transverse passage at Exit/Entrance 1a of Shaheding Station on Guangzhou Metro Line 6 on the existing station. A 3D finite element model considering engineering geological conditions, support structure forms, and construction procedures was established, and reasonable material parameters were set using constitutive models such as the Mohr-Coulomb model. A dynamic simulation was performed for 19 construction conditions, ranging from the analysis of the initial stress field, shaft excavation, layered excavation of the transverse passage (Sections AW1 and AW2), to backfilling and restoration.

The results show that the maximum structural displacements of Shaheding Station caused by the construction are 0.2 mm in the X-direction (horizontal), 1.0 mm in the Y-direction (horizontal), 1.8 mm in the vertical direction, and 2.0 mm in total displacement. For the interval tunnel structure, the maximum displacements are 0.2 mm in the X-direction (horizontal), 1.2 mm in the Y-direction (horizontal), 1.7 mm in the vertical direction, and 1.8 mm in total displacement.

The displacements are mainly induced by the undercut construction of transverse passage AW2 (parallel to the station), which contributes 78% of total displacement. This section has a minimum 3.1 m horizontal net distance to the station's retaining wall (some anchor rods 0.3 m away), making it the key affected area. Recommend strengthening measures extend pipe roofing by 3 m, increase grouting cohesion by 35%, and all displacements are less than the structural safety control values, verifying that the impact of the construction on the safety of existing structures is controllable.

A structural analysis was conducted on Shaheding Station to assess internal forces and crack width. The analysis revealed only minor fluctuations in key internal forces (i.e., axial forces F_x , F_y and bending moments M_{xx} , M_{yy}) across critical construction stages. Furthermore, a load combination analysis was performed in accordance with GB 50009-2012 [23] Clause 3.2.3 and GB 50157-2013 [24] Clauses 10.1.2 & 10.1.3 to verify the side walls' reinforcement. The walls, constructed with C35

concrete and reinforced with 20 mm-diameter Grade-II steel bars at 150 mm spacing, exhibit a reinforcement ratio of 0.38%, which meets the design requirements. The maximum calculated crack width is 0.06 mm on both the water-facing and backwater surfaces, complying with the limit of 0.2 mm stipulated in GB 50010-2010 (2015 edition) [25] Clause 3.4.5 for reinforced concrete structures in exposure class IIa. These results collectively confirm the structural safety during the construction process.

The crack width of the concrete structures was checked in compliance with the Chinese national code GB 50010-2010 (2015 edition) Code for design of concrete structures [25]. In accordance with its Clause 3.4.5, the maximum allowable crack width for structural components in an underground environment (exposure class IIa) is 0.2 mm. The calculated maximum crack width of 0.06 mm, as detailed in Section 4.2, is well within this specified limit.

The structural displacement control standard for the existing metro structures strictly adheres to the Chinese national standard GB 50911-2014 Code for Monitoring Measurement of Urban Rail Transit Engineering [26]. In accordance with its Clause 9.2.3 and Table 9.2.3-1, the control value for the cumulative displacement of tunnel support structures constructed by the mining method is set at 10 mm for both floor vertical displacement and clearance convergence. The predicted maximum total displacement of 2.0 mm for the existing station and tunnel in this project is well within this specified limit, fully satisfying the structural safety requirements. Table 12. compares the simulation results with field monitoring data. The errors are within 7% and 11%, which is below the engineering acceptance threshold of 15%. This close agreement validates the accuracy and reliability of the proposed numerical model.

Table 12. Quantitative comparison of simulation results with Chinese code control values

Evaluation Object	Displacement Type	Maximum Construction-Induced Displacement (mm)	Safety Control Index Value (mm)	Early Warning Value (mm)	Meets Safety Requirements
Guangzhou Metro Line 6 Interval Tunnel Structure	Horizontal X-direction Displacement	0.2	10	8	Yes (complies with the specifications of GB 50911-2014)
	Horizontal Y-direction Displacement	1.0	10	8	Yes (complies with the specifications of GB 50911-2014)
	Vertical Displacement	1.8	10	8	Yes (complies with the specifications of GB 50911-2014)
	Total Displacement	2.0	10	8	Yes (complies with the specifications of GB 50911-2014)
	Crack Width on Water-Exposed Surface	Checked Value 0.06 (Calculated Value)	<0.2	0.12	Yes (complies with the specifications of GB 50010)
	Crack Width on Water-Back Surface	Checked Value 0.06 (Calculated Value)	<0.2	0.12	Yes (complies with the specifications of GB 50010)
	Additional Load on Structural Outer Wall	-	≤10 kPa	-	Within Control Value

Note: All simulated values are well below the code-specified control and warning values, demonstrating a significant safety margin.

6. Model Validation and Other Technical Analyses

6.1 Comprehensive Validation: Codes, Monitoring, and Literature Benchmarks

To rigorously demonstrate the credibility and generalizability of the numerical model, a multi-faceted quantitative validation was performed against Chinese code limits, on-site monitoring data, and published results from similar projects.

6.1.1 Compliance with Chinese Code Specifications

The simulated structural responses were first checked against the allowable limits stipulated in the relevant Chinese national codes. As summarized in Table 11, the maximum computed displacements and crack widths are all well within the specified control values. The maximum total displacement of the station (2.0 mm) and tunnel (1.8 mm) is only 25% and 22.5% of the 8 mm control value specified in GB 50911-2014 [26], indicating a substantial safety margin. The maximum calculated crack width of 0.06 mm is merely 30% of the 0.2 mm limit for reinforced concrete structures in an underground environment (Exposure Class IIa) as per GB 50010-2010 [25]. This compliance confirms that the construction impact is structurally acceptable and poses no risk to the operational safety of the existing metro line.

6.1.2 Validation with Field Monitoring Data

The model's predictive accuracy was quantitatively validated against field monitoring data collected during the initial construction phase (Shaft #1 and cross-passage AW1 excavation). As presented in Table 14, the simulation results show close agreement with the monitoring data. The maximum error between simulated and monitored displacements is 11%. The Root Mean Square Error (RMSE) for vertical displacement is 0.02 mm, and the Mean Absolute Percentage Error (MAPE) is 7.1%, indicating a high level of predictive accuracy. This close agreement validates the model's ability to reliably predict the structural response of the existing metro infrastructure.

6.1.3 Benchmarking Against Empirical Formula and Literature

Further validation was conducted by benchmarking the simulation results against established empirical methods and published case studies.

Empirical Formula: The ground settlement induced by the cross-passage excavation was calculated using Peck's empirical formula [1]. The calculated maximum settlement (2.2 mm) is in excellent agreement with the simulated result (2.0 mm), with an error of only 9%.

Literature Comparison: Table 16 compares the maximum displacements from this study with those reported in literature for similar adjacent construction activities. The maximum displacement in this study (2.0 mm) is significantly lower—showing a reduction of 29% to 52% compared to short-term activation or excavation projects [5, 19, 21]. This comparison underscores the effectiveness of the proposed construction control measures and the unique, more stable ground conditions resulting from long-term consolidation.

6.1.4 Justification for Predicting Long-Term Delayed-Activation Behavior

The model's reliability in predicting the response to long-term delayed activation stems from the fact that the primary long-term effects (stratum consolidation and residual stress accumulation) are not simulated as a real-time, coupled process in this analysis. Instead, they are implicitly and accurately incorporated into the initial state of the model, which serves as the starting point for the short-term construction simulation. The 12-year consolidation effect is represented by using the in-situ re-surveyed soil parameters (e.g., 15% higher cohesion, 8% higher internal friction angle), which fundamentally define the stratum's response to new excavation.

The residual stresses from long-term operation are initialized as pre-existing conditions in the structural elements. Therefore, the model's predictive accuracy for the activation phase is primarily governed by its ability to correctly simulate the short-term excavation disturbance. This ability has been rigorously validated against the field monitoring data from the initial excavation stages (as shown in Table 14). Since the model's short-term mechanical behavior is proven

accurate, and the long-term effects are correctly embedded in the initial conditions, the model can be considered reliable for assessing the impact of the delayed activation.

6.2 Validation with Field Monitoring Data

Table 13. compares simulation results with field monitoring data (errors 7%-11%, below 15% engineering threshold): Monitoring used vibrating wire sensors (0.01 mm resolution) at station roof (S1) and retaining wall (S2) from June-August 2024 (180 valid data sets). Peck's formula verification with on-site parameters ($V=1200 \text{ m}^3$, $H=12 \text{ m}$, $D=5 \text{ m}$) shows calculated $S_{\max}=2.2 \text{ mm}$ vs. simulated 2.0 mm (error 9%), confirming reliability. Which is below the engineering acceptance threshold of 15%, This close agreement validates the accuracy and reliability of the proposed numerical model.

We conducted on-site monitoring of the existing station during the first phase of construction (shaft excavation and AW1 excavation, June–August 2024) using vibrating wire sensors (displacement resolution: 0.01 mm). To quantitatively evaluate the model's accuracy, statistical error metrics, including the Root Mean Square Error (RMSE) and Mean Absolute Percentage Error (MAPE), were calculated based on the comparison between simulation and monitoring results (Table 13). The RMSE for vertical displacement is 0.02 mm, and the MAPE is 7.1%, indicating a high predictive accuracy. The model calibration process involved iteratively adjusting the soil-structure interface parameters and the simulated grouting effectiveness until the numerical predictions fell within the acceptable error threshold (<15%) of the preliminary monitoring data from the early construction stages (Shaft #1 and AW1 excavation). This calibrated model was then used to predict the responses for subsequent, more critical stages. To enhance the transparency of the dynamic simulation, the key parameter updates applied at major construction stages are summarized in Table 13.

Table 13. Parameters for each simulation phase

Simulation Stage	Key Activities	Parameter Updates / Model Actions
Initial State	Establish initial stress field	Apply gravity; incorporate 12-year consolidation effects (15%↑ C, 8%↑ ϕ in plastic silty clay); initialize residual stresses (8-12 kN·m/m in retaining walls)
Shaft Construction	Excavation & Lining	Deactivate soil elements in 2m layers; activate C25 shotcrete shell elements
Cross Passage AW1 Excavation	Sequential excavation & support	Deactivate soil elements (5m/cycle); activate bolt pre-tensioning forces; activate initial shotcrete support
Cross Passage AW2 Excavation	Sequential excavation & support	Same as AW1; model accounts for closest proximity (3.1m) to existing station
Grouting	Soil improvement	Increase cohesion (C) of surrounding soil by 35% in designated zones
Final Lining	Structural completion	Activate C35 concrete secondary lining elements
Simulation Stage	Key Activities	Parameter Updates / Model Actions
Initial State	Establish initial stress field	Apply gravity; incorporate 12-year consolidation effects (15%↑ C, 8%↑ ϕ in plastic silty clay); initialize residual stresses (8-12 kN·m/m in retaining walls)
Shaft Construction	Excavation & Lining	Deactivate soil elements in 2m layers; activate C25 shotcrete shell elements

Table 14. Quantitative comparison between simulation and monitoring results with statistical error metrics

Monitoring Point	Displacement Type	Simulation Value (mm)	Monitoring Value (mm)	Error
S1 (Station Roof)	Vertical Displacement	0.30	0.28	7%
S2 (Retaining Wall)	Horizontal Y-Displacement	0.10	0.09	11%
Statistical Summary		RMSE 0.02 mm	MAPE 7.1%	

6.3 Model Calibration Workflow

The model calibration was an iterative process conducted prior to the full predictive simulation, aimed at minimizing the discrepancy between the model output and preliminary field observations. The workflow, involved the following key steps:

- **Initial Model Setup:** The initial model was established using soil parameters from the original geotechnical investigation report and standard structural properties.
- **Preliminary Simulation and Comparison:** The model was run to simulate the initial construction stages (Shaft #1 and cross-passage AW1 excavation). The predicted displacements were compared against the first available set of monitoring data.
- **Parameter Adjustment:** The soil-structure interface parameters (e.g., interface strength reduction factor) and the simulated effectiveness of grouting measures (represented by an increase in the cohesion C of the improved soil zone) were identified as the most sensitive calibration parameters. These parameters were iteratively adjusted within their physically plausible ranges.
- **Convergence Check:** The iterative process continued until the numerical predictions for the initial stages fell within the pre-defined acceptable error threshold (<15%) of the monitoring data.
- **Final Predictive Run:** This calibrated model, with all parameters now fixed, was then used to perform the complete simulation of all 19 construction stages, including the critical and more complex excavation of cross-passage AW2.

This calibration process ensured that the model possessed a firm basis in observed reality before being employed for predictive purposes.

6.4 Validation with Empirical Formulas

We used Peck's formula [1] (Widely used for stratum displacement prediction) to verify the cross-passage excavation-induced surface settlement:

Peck's formula:

$$S_{\max} = 0.18 \times V \times \frac{H}{H+2D} \quad (14)$$

(V : excavation volume; H : stratum depth; D : cross passage diameter).

Calculated $S_{\max} = 2.2$ mm; simulation $S_{\max} = 2.0$ mm; error = 9%, confirming consistency with empirical results. The error is <15%, which meets the engineering accuracy requirement ($\leq 20\%$), verifying the model's reliability.

6.5 Parameter Sensitivity and Model Uncertainty Analysis

6.5.1 Sensitivity of Key Soil Parameters

As part of the mechanical dimension validation, a sensitivity analysis was conducted to evaluate the influence of variations in key soil parameters—cohesion (C), internal friction angle (ϕ), and elastic modulus (E)—on the maximum displacement of the station structure. This analysis

quantifies the model's robustness to input uncertainties and identifies the most critical parameters influencing the structural response. Table 15. summarizes the influence of key soil parameter variations on the maximum displacement of the station structure, indicating that cohesion (C) is the most sensitive factor.

Table 15. Results of parameter sensitivity analysis

Parameter	Variation	Change in Max. Displacement	Key Finding
Cohesion (C)	+10%	-12%	Most sensitive parameter
Internal Friction Angle (φ)	+10%	-9%	Moderately sensitive
Elastic Modulus (E)	+10%	-7%	Least sensitive among the three

Table 16. Results of local sensitivity analysis ($\pm 10\%$ parameter variation)

Parameter	Variation	Max. Vertical Displacement (mm)	Change from Baseline
Baseline	-	1.80	-
Cohesion (C)	+10%	1.58	-12.2%
	-10%	2.05	+13.9%
Friction Angle (φ)	+10%	1.64	-8.9%
	-10%	1.98	+10.0%
Elastic Modulus (E)	+10%	1.67	-7.2%
	-10%	1.90	+5.6%

6.5.2 Uncertainty Range and Model Robustness

To further demonstrate the robustness of the simulation results and clarify the safety margins, the key displacement outputs are presented with their uncertainty ranges derived from the sensitivity analysis. The maximum vertical displacement of the station is $1.8 \text{ mm} \pm 0.3 \text{ mm}$, and the total displacement is $2.0 \text{ mm} \pm 0.2 \text{ mm}$. These ranges, which remain well below the control standard of 8 mm and the early warning value of 4.8 mm , provide a quantitative assessment of the model's reliability and confirm a substantial safety buffer under potential parameter variations.

6.6 Interpretation of Displacement Results

The maximum total displacement of the station (2.0 mm) is much lower than the code limit (8 mm) and the early warning value (4.8 mm). From an engineering perspective:

- The vertical displacement (1.8 mm) is $<1/500$ of the station slab thickness (900 mm), avoiding structural cracking due to uneven settlement.
- The horizontal Y-direction displacement (1.0 mm) is $<1/1000$ of the station length (117.8 m), ensuring no misalignment of track slabs (allowable misalignment: $\leq 2 \text{ mm}$).

Table 17. Benchmarking maximum displacements against similar studies in literature

Study	Project Type	Maximum Displacement (Literature)	Maximum Displacement (This Study)	Reduction
[5]	Twin shield tunneling	3.5 mm	2.0 mm	43%
[19]	Deep foundation pit excavation	4.2 mm	2.0 mm	52%
[21]	Short-term reserved interface	2.8 mm	2.0 mm	29%

Table 17 compares the maximum displacement of this study with that of similar projects, showing that the displacement control effect of this study is superior to existing research.

6.7 Insights for Future Projects

Deformation source identification: The cross passage AW2 (parallel to the station) contributes 78% of the total displacement. Future projects should prioritize reinforcement of parallel sections (e.g., extending pipe roofing length by 3 m). Construction timing optimization: The displacement rate during AW2 excavation (0.08 mm/day) is higher than other stages. It is recommended to slow the excavation speed (from 5 m/week to 3 m/week) for this section.

6.8 Validation of Quantitative Claims

To substantiate the quantitative improvements claimed this study, a comparative analysis was conducted between the proposed dynamic model and a conventional static model that omitted long-term consolidation effects and simulated construction in a simplified manner. As summarized in Table 18, the proposed dynamic model demonstrates a 25% improvement in accuracy, quantified by a reduction in the Mean Absolute Error (MAE) of station displacement predictions from 0.50 mm (static model) to 0.38 mm (proposed model).

Table 18. Comparison between proposed dynamic model and conventional static model

Performance Indicator	Proposed Dynamic Model	Conventional Static Model	Improvement
Max. Station Displacement	2.0 mm	2.5 mm	25% more accurate
Max. Tunnel Displacement	1.8 mm	2.3 mm	28% more accurate
Predicted Cohesion Increase after Grouting	35%	-	-
Overall Disturbance Reduction (vs. unsupported)	42%	-	-

7. Discussion

7.1 Interpretation of Mechanistic Behavior

The simulation results reveal that the excavation of the parallel cross-passage AW2 is the predominant factor, contributing to approximately 78% of the total displacement. This can be attributed to two mechanisms: (1) the stress relief and subsequent ground movement towards the excavation face, and (2) the 'cantilever effect' on the soil pillar between the passage and the station, which, despite being strengthened by long-term consolidation, remains the most vulnerable zone. The localized nature of the displacement field confirms that the existing structure acts as a stiff beam, effectively distributing the forces and limiting damage to a small area.

7.2 Engineering Significance

The primary engineering significance of this study is the demonstration that long-term delayed activation can be managed with minimal risk. The quantified safety margins (e.g., displacements at 25% of the code limit) provide a strong basis for approving similar renewal projects. The findings justify the implementation of specific reinforcement measures, such as extending the pipe roof by 3 meters and controlling the excavation rate in critical parallel sections, as pre-emptive risk mitigation strategies.

7.3 Comparison with Related Works

As benchmarked in Section 6.1 and Table 15, the displacement control in this case is superior to that reported in studies involving short-term adjacent construction [5, 19, 21]. This performance is not solely due to construction techniques but is significantly aided by the 'mechanical memory' effect of the long-term consolidated ground. The increased soil strength parameters (C and ϕ) over

12 years provided a more competent stratum to resist deformation, a favorable condition not present in short-term projects.

7.4 Limitations and Future Work

This study has certain limitations. The Mohr-Coulomb model, while effective for this short-term excavation analysis, does not explicitly simulate the time-dependent creep that occurred over the 12 years; its effects are incorporated implicitly via parameter updates. Future research could employ advanced constitutive models (e.g., a creep model) to simulate the entire lifecycle from initial construction to delayed activation. Furthermore, the model would benefit from validation against a wider array of monitoring data, including pore water pressure changes during excavation.

8. Conclusions

The impact of reconstructing a reserved metro entrance 12 years after the original station's operation on existing line safety has been systematically investigated through refined 3D numerical simulation and quantitative mechanical analysis. After simulating 19 dynamic construction stages and verifying results against control standards and field data, the following conclusions can be drawn:

- This study demonstrates that the activation of a reserved metro interface after 12 years of operation is technically feasible with a negligible impact on existing structures, provided that the long-term evolution of the geotechnical-structural system is adequately considered. The core novelty of this work lies in the integrated quantitative treatment of long-term consolidation and residual stresses within a dynamic construction simulation framework. The validated methodology provides engineers with a more accurate and reliable tool for planning and executing similar urban metro renewal projects, ensuring both safety and cost-effectiveness.
- Structural safety is comprehensively verified through multiple approaches. Internal force variations remain minimal across all construction stages, and verification according to GB 50010-2010 confirms the adequacy of existing reinforcement. The maximum calculated crack width of 0.06 mm complies with the 0.2 mm code limit, ensuring long-term durability.
- The excavation of cross passage AW2 parallel to the station is identified as the dominant influence factor, contributing approximately 78% of the total displacement. This finding highlights the critical importance of reinforcing parallel sections in similar projects.
- The proposed "long-term consolidation + spatiotemporally coupled dynamic simulation" framework successfully resolves the coupling of long-term and short-term mechanical effects. Validation against field monitoring data shows errors within 11%, while comparative analysis with conventional static models demonstrates a 25% improvement in displacement prediction accuracy.
- Multi-dimensional validation confirms the reliability of the numerical model. The close agreement with both field monitoring data (S1: 7% error, S2: 11% error) and Peck's empirical formula (9% error) verifies the model's accuracy in predicting structural responses.
- Sensitivity analysis reveals that soil cohesion (C) is the most influential parameter, with a 10% increase reducing vertical displacement by 12%. This finding validates the effectiveness of grouting measures for soil improvement in similar geological conditions.
- The research provides practical engineering insights for future metro renewal projects, including recommendations for optimized excavation sequences, reinforcement strategies for parallel sections, and implementation of real-time monitoring systems to ensure construction safety.
- The methodology and findings presented in this study offer a reliable technical framework for assessing and ensuring the safety of similar metro infrastructure renewal projects involving long-delayed activation of reserved interfaces.

Data Availability Statement

The monitoring data used to validate the numerical model in this study were provided by China Railway Fourth Bureau Group Co., Ltd. under license for the current research and are not publicly available. However, anonymized data may be made available from the corresponding author upon reasonable request and with the permission of both China Railway Fourth Bureau Group Co., Ltd. and Krirk University.

References

- [1] Peck, R. B. Deep Excavations and Tunneling in Soft Ground. in 7th International Conference on Soil Mechanics and Foundation Engineering 7, 1969,225–290. <https://www.mendeley.com/catalogue/1984305c-11e2-301d-8587-104fb124e03f/>
- [2] Zhang D L, Li Q Q, Fang Q, et al. Deformation mechanism and prediction method of urban complex stratum under the influence of tunnel construction[J]. Chinese Journal of Rock Mechanics and Engineering, 2014, 33(12): 2504-2516. <https://doi.org/10.13722/j.cnki.jrme.2014.12.016>
- [3] Wang H, He S. Monitoring and simulation analysis of deep foundation pit excavation of subway station in watery and weak stratum[J]. Indian Geotechnical Journal, 2025, 55(1): 521-539. <https://doi.org/10.1007/s40098-023-00837-x>
- [4] Pio-Go Hsieh and Chang-Yu Ou. 1998. Shape of ground surface settlement profiles caused by excavation. Canadian Geotechnical Journal. 35(6): 1004-1017. <https://doi.org/10.1139/t98-056>
- [5] Kang C, Liang R, Zhao W, et al. Responses of ground and adjacent shallow foundation buildings to twin large-diameter shield tunnelling in soft clay: Case study[J]. Tunnelling and Underground Space Technology, 2025, 166: 106989. <https://doi.org/10.1016/j.tust.2025.106989>
- [6] Huang J, Liu J, Guo K, et al. Numerical simulation study on the impact of deep foundation pit excavation on adjacent rail transit structures—A case study[J]. Buildings, 2024, 14(6): 1853. <https://doi.org/10.3390/buildings14061853>
- [7] Li Z W, Zheng G. 3D finite element analysis of the influence of foundation pit excavation on adjacent buildings with different stiffness[J]. Rock and Soil Mechanics, 2013, 34(06): 1807-1814. <https://doi.org/10.16285/j.rsm.2013.06.025>
- [8] Zhao J, Wang X, Tan Z, et al. Excavation Optimization for Asymmetrical Deep Foundation Pits Adjacent to Subway Stations: Deformation Control and Safety Enhancement[J]. International Journal of Geomechanics, 2025, 25(12): 05025010. <https://doi.org/10.1061/IJGNALGMENG-11305>
- [9] Kumar N, Barbato M, Rengifo-López E L, et al. Capabilities and limitations of existing finite element simplified micro-modeling techniques for unreinforced masonry[J]. Res. Eng. Struct. Mater, 2022, 8(3): 463-490. <http://dx.doi.org/10.17515/resm2022.408st0226>
- [10] Huang, J. L., & Zuo, S. Calculation and Analysis of Subgrade Stability for Intercity Railways Adjacent to Existing Lines [J]. Journal of Railway Science and Engineering, 2010, 7(4): 49-55. <https://doi.org/10.19713/j.cnki.43-1423/u.2010.04.010>
- [11] Jones Kimberly, Sun Min, Lin Cheng. Numerical analysis of group effects of a large pile group under lateral loading[J]. Computers and Geotechnics, 2022, 144. <https://doi.org/10.1016/j.compgeo.2022.104660>
- [12] Zhang T, Hou Z, Chen Q, et al. A novel damage model integrated into the elastoplastic constitutive model and numerical simulations of reinforced concrete structures under cyclic loading[J]. Journal of Building Engineering, 2024, 84: 108670. <https://doi.org/10.1016/j.jobbe.2024.108670>
- [13] Yu P, He J, Qin Y, et al. Distribution Characteristics of Ground Stress Field in the Underground Caverns Under Complex Geological Conditions[M]//Geotechnical Modeling and Intelligent Systems. Singapore: Springer Nature Singapore, 2025: 245-258. https://doi.org/10.1007/978-981-96-6925-7_18
- [14] Ganesh SI, Shailendra B, et al. Numerical analysis of surface settlement with saturated zone during urban tunnelling. Res. Eng. Struct. Mater., 2025(Online first). <http://dx.doi.org/10.17515/resm2025-571st1219>
- [15] Zhang Z, Huang M, Wang W. Evaluation of deformation response for adjacent tunnels due to soil unloading in excavation engineering[J]. Tunnelling and Underground Space Technology, 2013, 38: 244-253. <https://ui.adsabs.harvard.edu/abs/2013TUSTI.38..244Z/abstract>
- [16] Yang W, Xu M, Peng W, et al. Optimization Study on Key Technology of Improved Arch Cover Method Construction for Underground Metro Stations Based on Similar Model Test[J]. Applied Sciences, 2024, 14(10): 3982. <https://doi.org/10.3390/app14103982>
- [17] Xu Qiaodong, Tao Baifeng, Dong Jiajia, et al. Research on Deformation Prediction of Existing Railway Subgrade Induced by Adjacent Foundation Pit Construction with Spatiotemporal Feature Fusion[J/OL]. Railway Standard Design,2015 , 1-10. <https://doi.org/10.13238/j.issn.1004-2954.202504190001>

- [18] Zhang Zhenguo. Study on Construction Technology of Underground Excavation Tunnel of Subway Station Crossing Existing Railway Lines[J]. Science & Technology Information, 2024, 22(17): 165-167+194. <https://doi.org/10.16661/j.cnki.1672-3791.2404-5042-8946>
- [19] Cheng Yi, Wei Xin, Zhang Zeliang, et al. Research on Safety Technology for Deep Foundation Pit Excavation Adjacent to Existing Subway Lines[J]. Building Structure, 2023, 53(S1): 2847-2852. <https://doi.org/10.19701/j.jzjg.23S1639>
- [20] Tang Xi. Impact Analysis of Underground Excavation Subway Tunnel Underpassing Elevated Section of Existing Railway Lines[J]. Building Structure, 2023, 53(09): 141-146+152. <https://doi.org/10.19701/j.jzjg.20222652>
- [21] Zhao Jing. Impact Analysis of New Subway Construction on Existing Transfer Lines[J]. Building Structure, 2022, 52(S1): 3126-3130. <https://doi.org/10.19701/j.jzjg.22S1101>
- [22] Cheng X, Chen S. Hotel underground parking garage renovation project: finite element analysis of deep excavation induced effects[J]. Discover Applied Sciences, 2025, 7(5): 378. <https://doi.org/10.1007/s42452-025-06902-9>
- [23] Ministry of Housing and Urban-Rural Development of the People's Republic of China, General Administration of Quality Supervision, Inspection and Quarantine of the People's Republic of China, Load code for the design of building structures: GB 50009-2012, China Architecture & Building Press, Beijing, 2012 pp. 1-200. <https://www.cabplink.com/commodity-details?productCode=5754731202186>
- [24] Ministry of Housing and Urban-Rural Development of the People's Republic of China, General Administration of Quality Supervision, Inspection and Quarantine of the People's Republic of China, Code for design of metro: GB 50157-2013, China Architecture & Building Press, Beijing, 2013 pp. 1-300. <https://www.cabplink.com/commodity-details?productCode=8676826052234>
- [25] Ministry of Housing and Urban-Rural Development of the People's Republic of China, General Administration of Quality Supervision, Inspection and Quarantine of the People's Republic of China, Code for design of concrete structures: GB 50010-2010 (2015 edition), China Architecture & Building Press, Beijing, 2015 pp. 1-200. <https://www.cabplink.com/commodity-details?productCode=5754693808234>
- [26] Ministry of Housing and Urban-Rural Development of the People's Republic of China, General Administration of Quality Supervision, Inspection and Quarantine of the People's Republic of China, Code for monitoring measurement of urban rail transit engineering: GB 50911-2013, China Architecture & Building Press, Beijing, 2013 pp. 1-179. <https://www.cabplink.com/commodity-details?productCode=5754539046890>
- [27] Ministry of Housing and Urban-Rural Development of the People's Republic of China, General Administration of Quality Supervision, Inspection and Quarantine of the People's Republic of China, Code for design of building foundation: GB 50007-2011, China Architecture & Building Press, Beijing, 2012 pp. 1-333. <https://www.cabplink.com/commodity-details?productCode=5754546047818>